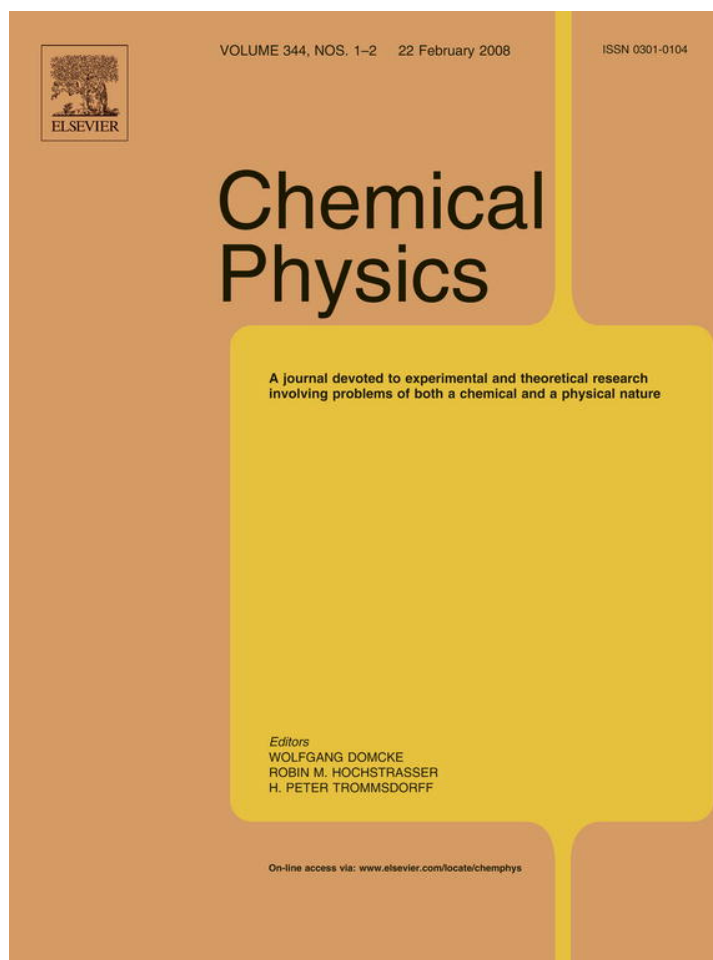


Provided for non-commercial research and education use.
Not for reproduction, distribution or commercial use.



This article was published in an Elsevier journal. The attached copy is furnished to the author for non-commercial research and education use, including for instruction at the author's institution, sharing with colleagues and providing to institution administration.

Other uses, including reproduction and distribution, or selling or licensing copies, or posting to personal, institutional or third party websites are prohibited.

In most cases authors are permitted to post their version of the article (e.g. in Word or Tex form) to their personal website or institutional repository. Authors requiring further information regarding Elsevier's archiving and manuscript policies are encouraged to visit:

<http://www.elsevier.com/copyright>



VUV absorption spectroscopy of acetonitrile between 7 and 20 eV: A revisionist study

Sydney Leach^{a,*}, Martin Schwell^b, Sun Un^c, Hans-Werner Jochims^d, Helmut Baumgärtel^d

^a *LERMA – UMR 8112, Observatoire de Paris-Meudon, 5, Place Jules Janssen, 92195 Meudon, France*

^b *Laboratoire Interuniversitaire des Systèmes Atmosphériques (LISA), Université Paris 7 et 12, 61 Avenue du Général de Gaulle, 94010 Creteil Cedex, France*

^c *Service de Bioénergetique, Biologie Structurale et Mécanismes, Institut de Biologie et Technologies de Saclay, CNRS-URA 2096, CEA Saclay, 91191 Gif-sur-Yvette, France*

^d *Institut für Physikalische und Theoretische Chemie der Freien Universität Berlin, Takustr. 3, 14195 Berlin, Germany*

Received 19 September 2007; accepted 11 December 2007

Available online 23 December 2007

Abstract

The VUV absorption spectrum of acetonitrile between 7 and 20 eV was obtained at high resolution using monochromatised Kr lamp radiation and synchrotron radiation as photon excitation sources. Absorption cross sections were measured over the spectral range studied. We have reinterpreted or assigned for the first time the bands of four valence transitions in the 7–12 eV region, aided by M.O. calculations of transition energies and oscillator strengths. These assignments also required consideration of vibronic symmetry conditions in electronic transitions not previously discussed in the context of the interpretation of acetonitrile VUV absorption spectra. Considerable revision of previously assigned Rydberg transitions converging to the ground 1^2E and first excited 1^2A_1 states of the cation in the 8.9–13.2 eV region was also effected. The vibrational modes and frequencies in the valence and Rydberg states and their relation to bonding characteristics of the molecular orbitals are discussed in detail. Absorption features in the 14.2–15.4 eV higher energy region, probably involve Rydberg transitions converging to the 2^2E ion state at 15.133 eV.

© 2007 Elsevier B.V. All rights reserved.

Keywords: Acetonitrile; VUV absorption spectroscopy; Valence transitions; Rydberg transitions

1. Introduction

Acetonitrile, CH_3CN , is one of the possible building blocks of biomolecules [1]. It has been observed by radioastronomy in several sites of the interstellar medium [2–4], in comets [5,6], (its release on the Deep Impact encounter with comet 9P/Tempel 1, has been suggested by I.R. emission spectroscopy [7]), and in the atmosphere of Titan [8,9]. Acetonitrile has also been detected in the Earth's stratosphere [10] and troposphere [11]. The VUV spectroscopy and photophysics of acetonitrile, which inform on the possibilities of photodestruction and photoionization processes, are thus of direct interest for exobiology and for

atmospheric studies of the Earth and other Solar system objects as well as for localising radioastronomy or infrared searches of CH_3CN in protected astrophysical sites.

In the present work we have measured the absorption spectrum of acetonitrile between 6 and 20 eV. The results are compared with spectra reported earlier. Molecular orbital calculations and a consideration of vibronic symmetry conditions in electronic transitions have led us to revise previous valence transition assignments, to renew assignments of Rydberg bands converging to the ground and first excited state of the acetonitrile cation and to suggest assignments of higher energy spectral features. The spectral analysis is useful for interpretation of photophysical studies reported elsewhere on fluorescence and photoionization quantum yield measurements on acetonitrile over the photon excitation range 8–22 eV [12]. A brief preliminary report on this work has been given previously [13].

* Corresponding author. Tel.: +33 1 4507 7561; fax: +33 1 4507 7100.
E-mail address: sydney.leach@obspm.fr (S. Leach).

2. Experimental

Absorption spectra of acetonitrile were measured with an experimental set-up whose essential components and operational procedure have been described previously [14] so that only a brief resume is given here. Monochromatised synchrotron radiation was obtained from the Berlin electron storage ring BESSY I (multi-bunch mode) in association with a M-225 McPherson monochromator modified to have a focal length of 1.5 m, and a gold coated spherical diffraction grating having 1200 lines/mm. Spectral dispersion was 5.6 Å/mm. The mean geometric slit width was 0.1 mm. The 30 cm long absorption cell is separated from the monochromator vacuum by a 1 mm thick stainless steel microchannel plate (MCP). Acetonitrile gas pressures were in the range 20–30 μbar, measured with a Balzers capacitance manometer. The small pressure gradient inside the absorption cell, due to the gas leak through the MCP, does not significantly affect the optical density measurements. The use of the MCP enables us to know the precise optical pathlength, the pressure drop being by a factor of the order of 1000, which ensures linearity in the Beer–Lambert analysis of the optical density measurements. VUV light transmission efficiency of the MCP is estimated to be about 10% and the transmitted light was largely sufficient for absorption measurements. Transmitted radiation strikes a window covered with a layer of sodium salicylate whose ensuing fluorescence was detected by a photomultiplier. We remark that the use of a laminar-type grating results in a very low (only few percent) contribution to second order radiation in the 10–20 eV region. Second order effects will be also very low below 10 eV because the gas column in the absorption cell reduces high energy radiation transmission much more than the low energy part.

Two scans, one with and one without acetonitrile gas, were carried out for determining the absorption spectrum. During a scan, the VUV light intensity falls off slightly due to continuous loss of electrons in the storage ring. The incident light intensity is furthermore a function of the energy-dependent reflectance of the diffraction grating. These two factors have been taken into account in normalisation of the spectra, which were recorded with a bandwidth of 0.05 nm. The precision of the energy scale is ±5 meV. Commercial CH₃CN of highest available purity grade was used, without further purification. The absorption spectra were measured three times, once with an energy interval of 5 meV, twice with an interval of 9 meV. The results were perfectly reproducible, with a slightly better resolution in the 5 meV step case.

After the 7–20 eV absorption study was made in 1999 with a synchrotron source, we carried out, in 2000, absorption measurements on CH₃CN, between 125 and 165 nm (7.5–10 eV), using a Kr microwave excited lamp to provide background radiation. These measurements, on highest purity acetonitrile, were made at three gas pressures, which we denote as low, medium and high, whose estimated values are 0.3, 3 and 15 torr, respectively. The wavelength

resolution was 0.05 nm. The monochromator was a 1-m McPherson M225 with a 1200 lines/mm classically ruled grating with Al-coating. The nominal dispersion of the instrument was 8.33 Å/mm yielding a resolution of 0.05 nm. The lamp was a commercial product from OPHTHOS, USA, filled with medium pressure (50 torr) Krypton and sealed by a LiF window. Lamp excitation was by an OPHTHOS microwave generator with 20 W typical electrical power. The absorption cell, 3.5 cm in length, was closed with LiF windows. The monochromator drive was continuous (no stepper motor) and perfect synchronization was guaranteed by synchronous motors in the monochromator and the recorder. A typical scan needed about 20 min each. Wavelength calibration was made with a 254 nm emission Hg source as well as OI emission peaks in the 130 nm region. The acetonitrile sample was freshly purified material.

3. Quantum chemical calculations

Acetonitrile is a symmetric top, having threefold symmetry about the molecular axis. It thus belongs to the C_{3v} symmetry group. Quantum chemical calculations were carried out using GAUSSIAN 03, Revision C.02 [15]. An initial geometry optimization of acetonitrile was performed using the hybrid density functional B3LYP and 6-311++G(3DF,3PD) basis set. “Tight” convergence criteria were used. Normal mode analysis confirmed that the final optimized geometry was a true potential energy minimum. The calculated structural parameters are in satisfactory agreement with gas phase experimental substitution structures, in parentheses, determined by electron diffraction and microwave spectroscopy [16]: bondlengths in nm, angles in degrees: C–C 0.1455 (0.1458), C≡N 0.11493 (0.11571), C–H 0.1089 (0.1036), ∠HCC 110.175, 110.170, 110.172 (109.45). The energies and oscillator strengths of transitions to the first 40 electronic excited states were calculated using the time-dependent DFT method [17] with the same hybrid density function and basis set. The unrestricted, spin-free, calculations provided triplet as well as singlet state information. The calculations are not expected to provide good values for transition energies beyond about 9–10 eV in the case of acetonitrile, since the eigenvalues are critically dependent on M.O. energy differences in time-dependent DFT calculations. However, these calculations differentiate well between strong and weak electronic transitions, thus facilitating the valence transition assignments.

4. Results and discussion

4.1. Theoretical preliminaries

We begin with a short discussion of the structure and electronic configurations of acetonitrile, and the nature and characteristics of the expected valence and Rydberg transitions, before presenting the experimental results.

Table 1
Comparison of experimental vertical ionization energies and calculated molecular orbital energies (eV)

M.O.	Expt. ^a	Our calc.	[28] ^c	[29] ^d	[20] ^e	[30] ^f	[21] ^g	[21] ^h
1a ₁	405.6	389.51	424.49	427.46	424.29			
2a ₁	292.98	278.30	307.58	312.38	307.71			
3a ₁	292.44	277.99	307.25	309.29	307.61			
4a ₁	29.7	24.92	34.10	35.11	33.04	31.68	31.85	25.97
5a ₁	24.9	21.39	28.38	28.94	28.08	26.89	25.90	23.16
6a ₁	17.4	17.24	18.89	19.74	18.84	17.48	17.08	16.88
1e	15.7	15.84	17.13	17.78	17.02	16.16	15.85	15.30
7a ₁	13.1	13.03	15.00	15.86	15.07	12.71	13.07	13.10
2e	12.20	11.85 ^b	12.73	14.03	12.60	10.97	12.23	12.17

^a Inner shell orbitals [27], valence orbitals [21].

^b See text.

^c SCF, Gaussian basis set.

^d LCAO-MO-SCF.

^e SCF.

^f Ab initio method.

^g Green's function method.

^h HAM/3.

Ground state acetonitrile has been determined by electron diffraction and by microwave spectroscopy [16,18] to belong to the C_{3v} symmetry group. Based on photoelectron spectroscopy [19–21], and on M.O. calculations [20–24] the electron configuration has been established as $\dots 6a_1^2(1e)^4(7a_1)^2(2e)^4$ and the ground state is 1^1A_1 . The 3e orbital is the LUMO and the 8a₁ LUMO + 1 orbital is estimated to lie 2.88 eV above it [25]. The calculated energies of the occupied M.O.s are given in Table 1, where they are compared with experimental vertical ionization energies determined by HeI and HeII photoelectron spectroscopy for valence electrons as well as, for inner shell ionizations, with the results of electron energy loss spectroscopy [26].

There is satisfactory agreement between our calculated valence shell orbital energies and the experimental ionization energies. A specific calculation of the total energy of the ground state of the acetonitrile cation provided a value of 11.85 eV for the ionization energy, in reasonable agreement with the experimental 12.20 eV. The calculated 4a₁ and 5a₁ orbital energies fall about 4 eV short of the respective experimental values 24.9 and 29.7 eV; these correspond to broad PES bands in a region where satellite lines become important [21], expressing extensive configuration interaction. Table 1 also includes the results of molecular orbital energy calculations by a variety of methods. The closest results to experimental valence shell ionization energies (the comparison being within the confines of Koopmans' approximation) are those of Åsbrink et al. using Green's function and the semiempirical HAM/3 (hydrogenic atoms in molecules) methods [21]. The inner shell orbitals are mainly 1s atomic orbitals and our calculated energies are about 15 eV below the experimental values, the difference being probably due to core hole effects. The SCF calculations of other authors [20,28,29] overestimate the inner shell M.O. energies by 15–20 eV (Table 1). The difference with our inner shell results probably reflects differences in

electron populations of the innermost atomic orbitals and differences in the mixing between valence and core molecular orbitals.

The photoelectron spectra and associated molecular orbital calculations [19–24] have led, in the past, to the following bonding characteristics of the following three occupied valence M.O.s and the two initially unoccupied M.O.s with which we will be concerned in this study:

2e: C≡N_π bonding (π_{CN}), C–C bonding, C–H antibonding

7a₁: N lone pair (σ_{CN})

1e: pseudo- π_{CH_3} , C–C bonding, C–H antibonding [19].

The 1e M.O. must be a π orbital since it is not observed by XPS [31,32].

The 3e LUMO is a π^* orbital, C–N antibonding, and the 8a₁ LUMO + 1 is a σ^* orbital, antibonding C–C and/or C–H [25].

The bonding characteristics of these molecular orbitals will be considered in more detail when we discuss later the vibrational frequencies observed in the excited electronic states of acetonitrile and in the electronic states of the cation. This will be seen to lead to revision of the bonding characteristics of some of these M.O.'s.

The singlet–singlet (and singlet–triplet in EELS experiments) valence transitions discussed in the literature [33–36] have been considered to involve principally 2e→3e ($\pi \rightarrow \pi^*$) and 7a₁→3e ($n_N \rightarrow \pi^*$) orbital promotions. The results of our calculations of optical transition energies (Tables 2 and 3) make it judicious to consider some other possible transitions, in particular $\pi \rightarrow \sigma^*$, involving 2e→8a₁ promotion, and $n \rightarrow \sigma^*$ (7a₁→8a₁) which have not previously been discussed. From the lowest energy $\pi \rightarrow \pi^*$ transition energy, 5.5 eV [36] and the $\pi^* - \sigma^*$ interval, 2.82 eV [26], we predict a 2e→8a₁, $\pi \rightarrow \sigma^*$ transition to occur at about 8.32 eV. Edard et al. [25] estimate the

Table 2
Calculated excited singlet state energies and transition oscillator strengths

State symmetry and number	Energy (eV)	Oscillator strength f	Principal orbital transitions	Transition type
1^1A_2	7.7926 (8.3) ^a	0.0	$2e \rightarrow 3e$	$\pi-\pi^*$
1^1E	7.8255	0.0018	$2e \rightarrow 8a_1$	$\pi-\sigma^*$
2^1E	8.0374 (8.8)	0.0036	$2e \rightarrow 3e$	$\pi-\pi^*$
2^1A_1	8.7542	0.0201	$7a_1 \rightarrow 8a_1$	$n-\sigma^*$
3^1A_1	9.0637 (11.9)	0.0918	$2e \rightarrow 3e$	$\pi-\pi^*$
3^1E	9.1699	0.0026	$2e \rightarrow 4e$	
2^1A_2	9.1893	0.0	$2e \rightarrow 4e$	
4^1E	9.2545 (10.1)	0.19	$7a_1 \rightarrow 3e$	$n-\pi^*$
5^1E	9.2864	0.016	$2e \rightarrow 9a_1$ $7a_1 \rightarrow 3e$	
6^1E	10.1287	0.003	$2e \rightarrow 9a_1$ $7a_1 \rightarrow 4e$	
4^1A_1	10.1372	0.0957	$7a_1 \rightarrow 9a_1$	
7^1E	10.3951	0.0262	$2e \rightarrow 10a_1$	
5^1A_1	10.4587	0.0586	$2e \rightarrow 4e$	

^a In parentheses, HAM/3 calculated energies [33].

Table 3
Calculated excited triplet state energies

State symmetry and number	Energy (eV)	Principal orbital transitions	Transition type
1^3A_1	6.058 (7.2) ^a	$2e \rightarrow 3e$	$\pi-\pi^*$
1^3E	6.784 (7.8)	$2e \rightarrow 3e$	$\pi-\pi^*$
2^3E	7.7125	$2e \rightarrow 8a_1$	$\pi-\sigma^*$
1^3A_2	7.7896 (8.3)	$2e \rightarrow 3e$	$\pi-\pi^*$
3^3E	7.8651	$7a_1 \rightarrow 3e$	$n-\pi^*$
2^3A_1	8.7019	$7a_1 \rightarrow 8a_1$	$n-\sigma^*$
2^3A_2	9.0524	$2e \rightarrow 4e$	
4^3E	9.1076	$2e \rightarrow 4e$	
3^3A_1	9.1904	$2e \rightarrow 4e$	
5^3E	9.2016	$2e \rightarrow 9a_1$	
4^3A_1	10.0136	$7a_1 \rightarrow 9a_1$	
6^3E	10.0469	$7a_1 \rightarrow 4e$	
7^3E	10.2505	$2e \rightarrow 10a_1$	

^a In parentheses, HAM/3 calculated energies [33].

$\pi-\sigma^*$ interval to be 8.21 eV, whereas our M.O. calculations give a value of 7.826 eV for the $1^1E \leftarrow 1^1A_1$ electronic state transition involving $2e \rightarrow 8a_1$ promotion (Table 2). The $n \rightarrow \sigma^*$ transition ($7a_1 \rightarrow 8a_1$, $2^1A_1 \leftarrow 1^1A_1$) is predicted to be at 9.14 eV from the data of Edard et al. [25]. Our electronic state calculations give a value of 8.754 eV. All of these transitions will be discussed below.

The symmetries of the electronic states that can occur for the C_{3v} molecule acetonitrile are A_1 , A_2 and E. The 1^1A_1 ground state is totally symmetric. An electric dipole transition $1^1A_2 \leftarrow 1^1A_1$ is forbidden in the C_{3v} symmetry group but a transition could occur, via the Herzberg–Teller vibronic coupling effect, if a nontotally symmetric vibration

of adequate symmetry was excited, especially if allowed electronic states are nearby. Transitions $1^1A_1 \leftarrow 1^1A_1$ and $1^1E \leftarrow 1^1A_1$ are dipole allowed.

We now consider which symmetry classes of vibration can be associated with the various electronic transitions mentioned above [37]. Acetonitrile has eight vibrational modes, four of which are totally symmetric (a_1) and four doubly degenerate (e). The electric dipole allowed transitions can have associated single or multiple quanta of a_1 modes. The $1^1A_1 \leftarrow 1^1A_1$ transitions can, in addition, have excited even numbers of quanta of the doubly degenerate e mode vibrations, giving rise to weak vibronic bands. The doubly degenerate 1^1E state can be subject to Jahn–Teller splitting of the vibronic levels in which e mode vibrations are excited, including both even and odd quanta, i.e. due to vibronic interactions within the 1^1E state itself. The forbidden $1^1A_2 \leftarrow 1^1A_1$ transition can appear via excitation of a single quantum of an e mode vibration (Herzberg–Teller effect, i.e. vibronic interactions with another electronic state, of 1^1A_1 or 1^1E symmetry), accompanied by single or multiple quanta of a_1 mode vibrations. Vibrations excited in $1^1A_1 \leftarrow 1^1A_1$ transitions should have normal anharmonic behaviour, but $1^1E \leftarrow 1^1A_1$ transitions subject to Jahn–Teller splitting of the vibronic levels could exhibit irregular vibrational intervals in the absorption spectrum. The degree of irregularity will depend on the strength of the Jahn–Teller vibronic coupling.

The C_{3v} symmetry of acetonitrile allows, in principle, the following six *ns*, *np* and *nd* Rydberg series: *nsa*₁, *npa*₁, *npe*, *nda*₁, *nde*(1), *nde*(2), i.e. in linear $C_{\infty v}$ symmetry, *nσ*, *npσ*, *npπ*, *ndσ*, *ndπ*, *ndδ*, often used in discussions of acetonitrile Rydberg states [33–36,38]. Rydberg states converging to the ground and first excited electronic states of the cation are expected to conserve C_{3v} nuclear symmetry and thus have A_1 , A_2 or E electronic state symmetry.

4.2. Absorption spectra: observations

Fig. 1 shows an overall absorption spectrum of acetonitrile between 7 and 20 eV. The most structured part of the spectrum is in the 9–13 eV region. In Fig. 2 we show the absorption spectrum in the 125–165 nm (9.92–7.51 eV) region, observed at “low”, “medium” and “high” pressures, using a microwave excited Kr lamp to provide the background continuum. The peak wavelengths can easily be read off these recorder chart spectra, which include the base line corresponding to $\log I(0)$. The “negative peaks” seen in the low pressure and base line spectra in the 130 nm region are due to OI resonance line emissions present in the Kr source. They can be used to calibrate the wavelength scale.

Our spectra show considerable structure, more detailed than in the spectrum reported by Nuth and Glicker [38], who published the only other high resolution study of acetonitrile absorption over the whole 7–20 eV spectral region that we have studied; (a compressed absorption spectrum over the range 8.3–41.3 eV was published,

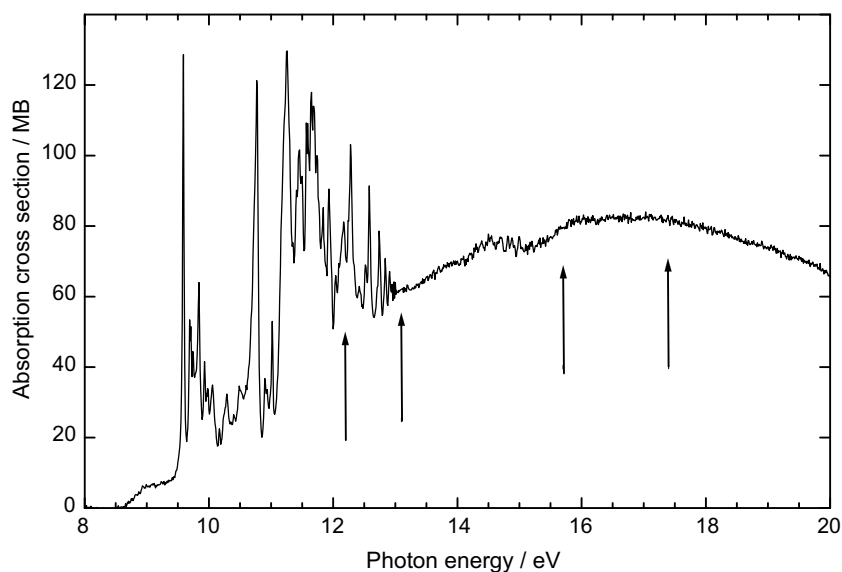


Fig. 1. Overview of the absorption spectrum of acetonitrile between 8 and 20 eV. Vertical arrows indicate ionization energies.

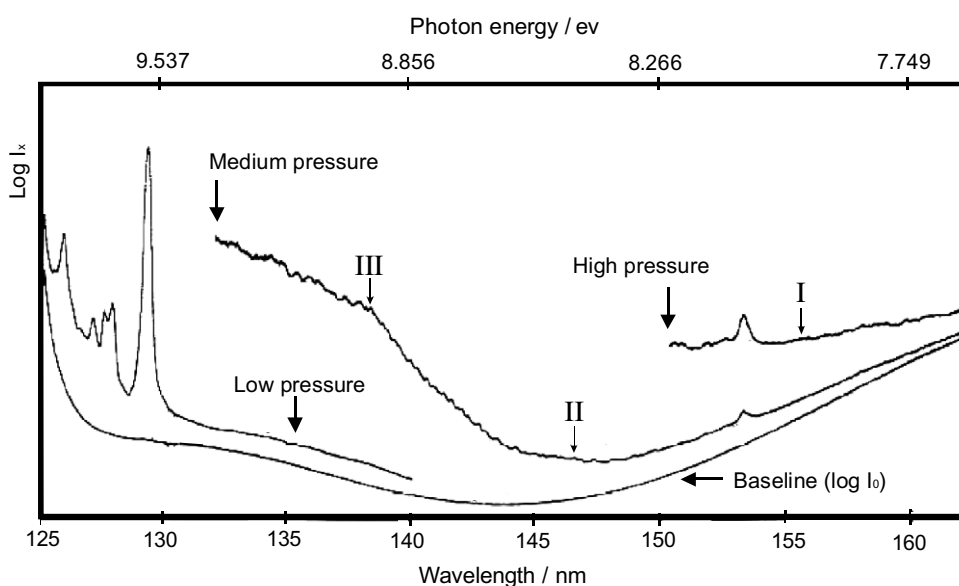


Fig. 2. Absorption spectrum of acetonitrile in the 125–165 nm (9.92–7.51 eV) region, observed at “low”, “medium” and “high” pressures (see text). I, II and III arrows indicate the O_0^0 origin bands of the valence transitions $1^1E \leftarrow 1^1A_1$, $2^1E \leftarrow 1^1A_1$ and $2^1A_1 \leftarrow 1^1A_1$, respectively.

without quantitative absorption peak energy data, by Kanda et al. [39]). The spectra which we obtained are also consistent with the earlier photographic absorption spectra of acetonitrile published by Herzberg and Scheibe [40] (up to 8 eV) and by Cutler [41] (6.9–12.4 eV) as well as more recent absorption studies, also over more limited spectral ranges than ours, by Suto and Lee [42] (6.9–11.7 eV) and Eden et al. [35] (3.9–10.8 eV).

From the relative intensities of strong narrow absorption bands it is clear that our spectral resolution is higher than that of Nuth and Glicker [38], who quoted a resolution of 0.05 nm over the 7.75–20.66 eV range, measured with data point intervals of 0.02 nm (2.5 meV at 100 nm).

In general, published absorption cross sections are given to within an uncertainty of 10%. Our peak absorption cross sections are similar to those of Nuth and Glicker [38] and of Eden et al. [35] over the common spectral ranges but are $20 \pm 5\%$ higher than those of Suto and Lee [42] and of Kanda et al. [39]. This difference is possibly related to a lower spectral resolution, 0.08 nm [42], 0.10 nm [39] than our 0.05 nm.

Since our initial measurements were made with a synchrotron radiation source, and were the subject of a preliminary publication [13], an absorption spectrum of acetonitrile over the 3.9–10.8 eV region has been reported by Eden et al. [35], who also used synchrotron radiation

as a photon source. Their resolution (FWHM) was 0.075 nm, corresponding to 1.5 meV over the energy range studied. In the measurements we made at three different pressures, we observe the same spectrum as Eden et al. over the common energy range (Table 4). In particular, there is a series of weak bands between 8 and 9.5 eV, observed at medium pressure, but virtually absent at low pressure, which appear to be slightly better resolved in our spectrum, even if the peak amplitudes are smaller in our case. The absorption cross sections of the bands between 8.1 and 9.4 eV are of the order of 0.2 mB above a continuous background whose cross section increases from 0.7 mB at 8 eV to about 8 mB at 9.4 eV. These bands were first published by Eden et al. [35]. Their observation in our study, using a different photon source, confirms their existence as features of acetonitrile absorption.

4.3. Valence transitions

Our peak energies in the 8–9.5 eV region, measured in the “medium pressure” spectrum, are compared with the results of Eden et al. [35] in Table 4. This spectral region contains the bulk of the valence transition bands. Table 4 also includes the energies of electron energy loss spectral (EELS) features reported by Rianda et al. [36] and by Gochel-Dupuis et al. [34] in this same energy region. Given the diffuseness reported by Eden et al. for many bands, indicated as (D) in Table 4, agreement between the two sets of bands is quite satisfactory. All the bands observed by Eden et al. in this spectral region were observed in our spectrum, except for a band they report at 8.06 eV which is possibly hidden in the red wing of the 8.093 eV band in our spectrum (Fig. 2), and two diffuse bands, at 9.41 and 9.47 eV, at the high energy limit of the weak band system, 9.47 eV being at the very limit of our medium pressure observations. On the other hand, we observed two bands, at 8.869 and 8.939 eV, not reported by Eden et al., and which could be components of unresolved features in their spectra.

Eden et al. [35] assigned most of the observed bands in the 8–8.9 eV region to vibrational components of two valence transitions, which we indicate as I and II in Table 4, associated with the orbital promotion $2e \rightarrow 3e$ ($\pi \rightarrow \pi^*$). They did not specify the symmetries of the excited electronic states. The three bands reported as unassigned by Eden et al. at 8.49, 8.71 and 8.756 eV, were observed in our spectrum, at 8.49, 8.716 and 8.759 eV, in good agreement with their observations, and are assigned in Table 4. Weak bands in the 8.9–9.5 eV region (Fig. 2), indicated as transition III in Table 4, observed also by Eden et al., were assigned by the latter to vibrational components of the ${}^1E \leftarrow {}^1A_1$ transition associated with the orbital promotion $7a_1 \rightarrow 3e$ ($n_N \rightarrow \pi^*$).

The peak at 8.093 eV in our spectrum is more prominent than the 8.09 eV band reported by Eden et al. as a weak diffuse structure. This peak is due partially to an acetone impurity, introduced by the cell cleaning procedure.

Several weaker bands of acetone were observed in the high pressure spectrum (Fig. 2), as indicated in Table 4.

4.3.1. Forbidden transitions

The “high pressure” spectrum (Fig. 2) also contains a few very weak bands below 8.0 eV, at 7.963, 7.922, 7.872, 7.847, 7.798, 7.781, 7.756, 7.739 and 7.715 eV. The 7.963 eV band may correspond to the 7.95 eV band observed in the EELS experiments of Gochel-Dupuis et al. [34], which they assigned as the origin band O_0^0 of a ($2e \rightarrow 3e$) $\pi \rightarrow \pi^*$ transition, adopted also by Eden et al. [35]. For reasons discussed below we have re-assigned it as the origin band of the $\pi \rightarrow \sigma^* {}^1E \leftarrow {}^1A_1$ transition (valence transition I, Table 4). This very weak band was not reported by Eden et al., whose published spectra in the same spectral region as our Fig. 2 are similar to our “medium pressure” spectrum. These authors considered the $\pi \rightarrow \pi^*$ transition origin band to be at 7.97 eV, on the basis of their vibrational analysis, thus following the assignment of Gochel-Dupuis et al. (Table 4).

The other eight bands between 7.715 and 7.922 eV in our high pressure spectrum are possibly vibrational structure components of the Herzberg–Teller induced ${}^1A_2 \leftarrow {}^1A_1$ $\pi \rightarrow \pi^*$ forbidden transition which is calculated to occur at 7.793 eV (Table 2) (see later). Another possibility is that they are components of singlet–triplet transition(s) reported to occur in this spectral region [34,36]. A band at 8.1 eV in electron energy loss spectra of acetonitrile observed by Rianda et al. [36] was assigned by them as a $\pi \rightarrow \pi^*$ singlet–triplet transition on the basis of the differential cross section observations as a function of scattering angle at an incident electron energy of 25 eV. Other, weaker, possible singlet–triplet transitions of acetonitrile, in the 5.2–7.5 eV region, are reported as broad bands by Rianda et al. [36], as well as by Gochel-Dupuis et al. [34] at 5.8 and 6.8 eV. These lower energy bands would not have been observable in our absorption spectra range. However, our calculated electronic transition energies indicate the existence of a series of triplet–singlet transitions starting at 6.06 eV (Table 3). The $2e \rightarrow 3e$ $\pi \rightarrow \pi^*$ triplet–singlet transitions are calculated to be at 6.06, 7.71 and 7.79 eV (Table 3). Five triplet–singlet transitions are calculated to occur between 6.06 and 7.87 eV. Another group of five spin forbidden transitions are calculated to occur between 8.70 and 9.20 eV (Table 3). Still higher energy singlet–triplet transitions are calculated to start at 10.01 eV. These would be entirely masked by strong valence and Rydberg transitions.

4.3.2. ${}^2E \leftarrow {}^1A_1$ $\pi \rightarrow \pi^*$, transition II, and ${}^3A_1 \leftarrow {}^1A_1$ $\pi \rightarrow \pi^*$, transition IV

In Table 4 we have re-assigned many of the bands assigned by Eden et al. as a result of the following discussion of the electronic and vibrational symmetries relevant to the optical transitions, aided also by our calculations of transition energies and oscillator strengths. As mentioned above, the symmetries of the excited singlet

Table 4
Absorption peak energies and valence transition assignments 7.9–9.5 eV

Peak energy (eV) Present study	Peak energy (eV) Eden et al. [35]	Band assignments Eden et al. [35]	Band assignments Present study
7.963 ^a	7.97 ^b	I(2e → 3e)π–π*O ₀ ⁰	I (2e → 8a ₁)π–σ* 1 ¹ E ← 1 ¹ A ₁ O ₀ ⁰
See text	8.06 (D) ^c	Iπ–π*8 ₀ ²	Iπ–σ*4 ₀ ¹
8.093	8.09 (D); 8.1 ^d	Iπ–π*3 ₀ ¹	Iπ–σ*3 ₀ ¹
8.133	8.14 (D)	Iπ–π*8 ₀ ⁴	Iπ–σ*4 ₀ ²
8.165			Acetone impurity
8.182	8.19 (D); 8.20 ^c	Iπ–π*2 ₀ ¹	Iπ–σ*2 ₀ ¹ ;
8.225	8.23 (D)	Iπ–π*3 ₀ ²	Iπ–σ*3 ₀ ²
8.239			Acetone impurity
8.28	8.277	Iπ–π*2 ₀ ¹ 8 ₀ ²	Iπ–σ*2 ₀ ¹ 4 ₀ ¹ ;
8.33	8.321	Iπ–π*1 ₀ ¹	Iπ–σ*1 ₀ ¹
			Iπ–σ*3 ₀ ¹
8.37	8.366	Iπ–π*2 ₀ ¹ 8 ₀ ⁴	Iπ–σ*2 ₀ ¹ 4 ₀ ²
8.42	8.411	Iπ–π*2 ₀ ²	Iπ–σ*2 ₀ ²
8.45	8.44 (D); 8.44 ^c	(2e → 3e)Ππ–π*O ₀ ⁰	Π (2e → 3e) π–π* 2 ¹ E ← 1 ¹ A ₁ O ₀ ⁰
8.46	8.46 (D); 8.45 ^d	Iπ–π*1 ₀ ¹ 3 ₀ ¹	Iπ–σ*1 ₀ ¹ 3 ₀ ¹
8.49	8.49		Iπ–σ*3 ₀ ⁴
8.50	8.51 (D)	Iπ–π*2 ₀ ² 8 ₀ ²	Iπ–σ*2 ₀ ² 4 ₀ ¹
8.53	8.527	Ππ–π*8 ₀ ²	Ππ–π*4 ₀ ¹
8.56			Acetone impurity
8.577	8.574	Iπ–π*1 ₀ ¹ 3 ₀ ²	Iπ–σ*1 ₀ ¹ 3 ₀ ²
			Ππ–π*3 ₀ ¹
8.601	8.598	Iπ–π*2 ₀ ² 8 ₀ ⁴	Iπ–σ*2 ₀ ² 4 ₀ ²
8.622	8.62 (D)	Ππ–π*8 ₀ ⁴	Ππ–π*4 ₀ ²
8.646	8.64 (D); 8.64 ^d	Iπ–π*2 ₀ ³	Iπ–σ*2 ₀ ³
8.676	8.66 (D); 8.66 ^c	Iπ–π*1 ₀ ²	Iπ–σ*1 ₀ ² ;
8.688	8.682	Ππ–π*2 ₀ ¹	Ππ–π*2 ₀ ¹
8.716	8.71; 8.72 ^d		Ππ–π*3 ₀ ¹
8.730	8.731	Iπ–π*2 ₀ ³ 8 ₀ ²	Iπ–σ*2 ₀ ³ 4 ₀ ¹
8.759	8.756		Ππ–π*2 ₀ ¹ 4 ₀ ¹
8.778	8.775	Ππ–π*2 ₀ ¹ 8 ₀ ²	Ππ–π*1 ₀ ¹
8.803	8.800	Iπ–π*1 ₀ ² 3 ₀ ¹	Iπ–σ*1 ₀ ² 3 ₀ ¹
8.821	8.818	Iπ–π*2 ₀ ³ 8 ₀ ⁴	Iπ–σ*2 ₀ ³ 4 ₀ ²
8.847	8.856	Iπ–π*2 ₀ ⁴	Iπ–σ*2 ₀ ⁴ ;
			Ππ–π*3 ₀ ³
8.869			Ππ–π*1 ₀ ¹ 4 ₀ ¹
8.894	8.88 (D)	Ππ–π*2 ₀ ¹ 8 ₀ ⁴	Ππ–π*2 ₀ ¹ 4 ₀ ²
8.907	8.92 (D)	Iπ–π*1 ₀ ² 3 ₀ ²	Iπ–σ*1 ₀ ² 3 ₀ ²
8.926	8.93 (D)	3sσO ₀ ⁰ ; Ππ–π*2 ₀ ²	Ππ–π*2 ₀ ²
8.939			Ππ–π*2 ₀ ³ 3 ₀ ²
8.968	8.965; 8.96 ^d ; 8.96 ^c	(7a ₁ → 3e)n _N –π*O ₀ ⁰	ΠΠ (7a ₁ → 8a ₁) n–σ* 2 ¹ A ₁ ← 1 ¹ A ₁ O ₀ ⁰
8.997	8.991	Iπ–π*1 ₀ ³	Iπ–π*1 ₀ ³
9.037	9.030	n _N –π*8 ₀ ²	Ππ–π*1 ₀ ¹ 3 ₀ ²
9.070	9.063	n _N –π*4 ₀ ¹	ΠΠn–σ*4 ₀ ¹
9.106	9.103; 9.11 ^d ; 9.10 ^c	n _N –π*8 ₀ ⁴	Ππ–π*1 ₀ ²
9.130	9.123	n _N –π*4 ₀ ¹ 8 ₀ ²	ΠΠn–σ*3 ₀ ¹
9.164	9.164	n _N –π*4 ₀ ²	ΠΠn–σ*4 ₀ ²
9.205	9.205; 9.21 ^d ; 9.20 ^c	n _N –π*4 ₀ ¹ 8 ₀ ⁴	ΠΠn–σ*2 ₀ ¹
9.235	9.232	n _N –π*4 ₀ ² 8 ₀ ²	ΠΠn–σ*3 ₀ ¹ 4 ₀ ¹
9.280	9.273	n _N –π*4 ₀ ³	ΠΠn–σ*4 ₀ ³
9.315	9.301; 9.30 ^c	n _N –π*4 ₀ ² 8 ₀ ⁴	ΠΠn–σ*1 ₀ ¹
9.336	9.34 (D)	n _N –π*4 ₀ ³ 8 ₀ ²	ΠΠn–σ*3 ₀ ¹ 4 ₀ ²
9.379	9.372	n _N –π*4 ₀ ⁴	ΠΠn–σ*4 ₀ ⁴
	9.41 (D)	n _N –π*4 ₀ ³ 8 ₀ ⁴	ΠΠn–σ*1 ₀ ¹ 4 ₀ ¹
9.432	9.44 (D)	n _N –π*4 ₀ ⁴ 8 ₀ ²	ΠΠn–σ*2 ₀ ²
	9.47 (D)	n _N –π*4 ₀ ⁵	Ππ–π*1 ₀ ³

^a Observed in our “high pressure” spectra (see text).

^b Not observed but derived by Eden et al. from their vibronic analysis [35].

^c (D) = classed as a diffuse band in [35].

^d Rianda et al. [36].

^e Gochel-Dupuis et al. [34].

electronic states that can arise from the orbital promotion $2e \rightarrow 3e$ are the two allowed states A_1 and E and the forbidden transition state A_2 . The results of the HAM/3 calculations of the energies of acetonitrile valence states by Fridh [33] and those of our own M.O. calculations (Table 2) predict that the lowest singlet $\pi\text{-}\pi^*$ excited state is 1A_2 and is followed by 1E and 1A_1 , in that energy order.

The Herzberg–Teller induced ${}^1A_2 \leftarrow {}^1A_1$ $\pi\text{-}\pi^*$ transition would only be expected to borrow sufficient intensity to be observed if strongly allowed states were close in energy to the excited state. Our calculations indicate that Herzberg–Teller vibronic coupling is unlikely to be important, so that either the induced transition is not observed or it is indeed assignable to the extremely weak features below 8 eV observed in the high pressure spectrum, as discussed above. The allowed $\pi\text{-}\pi^*$ ${}^2E \leftarrow {}^1A_1$ transition is predicted to be relatively weak ($f = 0.0036$) and to lie at higher energies (Table 2). We calculate it to occur at 8.037 eV (Table 2) and assign its O_0^0 origin to the observed transition II band at 8.45 eV.

The third member of the $2e \rightarrow 3e$ $\pi\text{-}\pi^*$ transitions, ${}^3A_1 \leftarrow {}^1A_1$ is calculated to occur at 9.06 eV, with an oscillator strength of 0.0918, i.e. 25 times as strong as the $\pi\text{-}\pi^*$ allowed ${}^2E \leftarrow {}^1A_1$ transition. HAM/3 calculations [33] predict 11.9 eV, so that it is reasonable to infer that it occurs in the region of strong absorption above 9.5 eV, possibly overlapping with some of the Rydberg transitions. The origin band of the ${}^3A_1 \leftarrow {}^1A_1$ transition is assigned to the strong 11.256 eV feature and this assignment is discussed in more detail later (Section 4.5.2). We will refer to ${}^3A_1 \leftarrow {}^1A_1$ as valence transition IV.

4.3.3. ${}^1E \leftarrow {}^1A_1$ $\pi\text{-}\sigma^*$, transition I

The $2e \rightarrow 8a_1$, ($\pi \rightarrow \sigma^*$) ${}^1E \leftarrow {}^1A_1$ valence transition which, as mentioned earlier, we predict to occur at about 7.83 eV, has a calculated oscillator strength (0.0018) compatible with the strength of the bands observed in the transition I region, whose origin band is at 7.963 eV, and which was previously assigned by Gochel-Dupuis et al. [34] and by Eden et al. [35] to a $2e \rightarrow 3e$ ($\pi \rightarrow \pi^*$) transition (Table 4).

4.3.4. ${}^2A_1 \leftarrow {}^1A_1$ $n\text{-}\sigma^*$, transition III

The $7a_1 \rightarrow 8a_1$, ($n \rightarrow \sigma^*$) ${}^2A_1 \leftarrow {}^1A_1$ transition origin is calculated to be at 8.752 eV, with an oscillator strength $f = 0.02$. We assign it to the 8.968 eV band, origin of the transition III. This f value is 5.6 times greater than that calculated for transition II ($\pi\text{-}\pi^*$ ${}^2E \leftarrow {}^1A_1$) and indeed the transition III bands are more intense than those of transition II (see below). We note that the 8.968 eV band was assigned by Gochel-Dupuis et al. [34] and Eden et al. [35] as the origin band of the ${}^4E \leftarrow {}^1A_1$ transition associated with the orbital promotion $7a_1 \rightarrow 3e$ ($n_N \rightarrow \pi^*$). This transition is calculated to occur at 9.255 eV (HAM/3 calculations give 10.1 eV [33]) and to be over 50 times stronger ($f = 0.19$) (Table 2) than the $\pi\text{-}\pi^*$ ${}^2E \leftarrow {}^1A_1$ transition ($f = 0.0036$). We consider that the $7a_1 \rightarrow 3e$ ($n_N \rightarrow \pi^*$) transition contributes to the strong background absorption

above 9.5 eV, along with $2e \rightarrow 3e$, ${}^3A_1 \leftarrow {}^1A_1$ $\pi\text{-}\pi^*$ transition, which is expected to occur at a higher energy, as discussed above.

We remark that the bands from 8.968 eV to 9.5 eV, which we re-assign to the $7a_1 \rightarrow 8a_1$, ($n \rightarrow \sigma^*$) ${}^2A_1 \leftarrow {}^1A_1$ valence transition, have FWHM $\approx 100 \text{ cm}^{-1}$ (13 meV). They are both more intense and broader than those at lower energies, whose FWHM are mainly of the order of 60 cm^{-1} . A comparison of the integrated peaks, above the continuous background absorption, in the two spectral regions is in agreement with the calculated relative intensities of the respective transitions. Furthermore, the FWHM values indicate that the 1E and 2E states are less predisposed than those of the 2A_1 state. These FWHM correspond to nonradiative relaxation rates of 1.1×10^{13} and $1.9 \times 10^{13} \text{ s}^{-1}$ for the respective excited states. These rates are such that fluorescence quantum yields of acetonitrile from these states should be extremely low, of the order of 1% or less, and indeed no fluorescence of the parent molecule has been reported. The electronic excited states under discussion must be almost completely dissociative, with the differences in the FWHM of the I, II and the III transition bands indicating the existence of non-uniform dissociation rates. We remark that Suto and Lee [42] consider the photodissociation cross section of acetonitrile to be equal to its photoabsorption cross section in the 6.89–11.7 eV region of their study, i.e. below the ionization limit. They observed that the fluorescence quantum yields of emitting fragments (e.g. CN, [12]) are of the order of 1% or less in the 8.968–9.5 eV spectral region [42].

4.3.5. Vibrational components of the valence transitions

Our re-assignments in Table 4 also include vibrational components of the electronic transitions. In their spectral analysis Eden et al. [35] considered, without discussion, that the doubly degenerate vibration ν_8 could be excited only in even numbers of quanta in the I, II and III transitions. They did not discuss the symmetry implications for excitation of vibrational modes. The restriction on excitation of the doubly degenerate mode 8 vibration figures very largely in their analysis of transitions I, II and III. In their assignments of bands in which mode 8 is excited in even numbers of quanta (8_0^2 and 8_0^4) in the electronic excited states, the average values of ν_8 are 45 meV (transition I), 46 meV (II) and 34 meV (III). The ground state frequency is 45 meV, so that Franck–Condon factors should render these 8_0^2 and 8_0^4 transitions of negligible intensity, at least in transitions I and II, and in any case they should be very weak with respect to bands in which totally symmetric vibrations are excited, in transition III. This is contrary to the observed relative intensities of the bands in which a_1 and e mode vibrations are separately excited. Furthermore there is no sign of vibrational interval irregularities or odd numbers of mode 8 excitations as might be expected for transitions to Jahn–Teller affected 1E states, yet two of the transitions I, II and III are expected to have 1E excited states. We were thus led to propose revisions not only of

the orbital and electronic symmetry assignments but also of many of their vibrational assignments. In particular, the bands of Eden et al. involving 8_0^2 and 8_0^4 excitations in transitions I and II are re-assigned to mode 4 excitations 4_0^1 and 4_0^2 , respectively. Our new assignments, given in the right-hand column of Table 4, take fully into consideration the symmetry properties of the vibronic transitions, as evoked and discussed above.

4.4. Vibrational frequencies in the valence states

The frequencies of the vibrational modes observed in the three valence transitions assigned in the 7.7–9.5 eV energy region, as well as the $3^1A_1 \leftarrow 1^1A_1$ valence transition in the 11.256–11.975 eV region (see later) are given in Table 5, where they are compared with the neutral ground state frequencies and the those of the ground and two excited electronic states of the acetonitrile cation. This leads to revision of some previously accepted bonding characteristics of the various molecular orbitals.

4.4.1. Mode 1

Mode 1 is a C–H stretching vibration whose neutral ground state frequency is 366 meV. It is little reduced on promoting a 2e electron to the $8a_1$ orbital, but decreases by about 10% in the $2e \rightarrow 3e$ excited 2^1E and 3^1A_1 valence states. The 2e orbital has previously been considered to be not only C≡N and C–C bonding but also as having some C–H antibonding character [19]. From the frequency behaviour it thus appears that the 2e M.O. is mildly C–H bonding, or that 3e is more C–H antibonding than 2e. We prefer the first interpretation, especially since ν_3 , the frequency of the CH_3 symmetric deformation mode is considerably reduced in the $\pi \rightarrow \pi^*$ transition excited states 2^1E and 3^1A_1 , the lowered deformation frequency being associated with the lengthening of the C–H bond.

In this connection we re-examine the high resolution photoelectron spectrum of acetonitrile measured by Gochel-Dupuis et al. [43], arguing that a C–H bonding 2e orbital should lead to excitation of ν_1 in the first PES band, where the 1^2E ground state of the ion is formed by ejection of a 2e M.O. electron. Such an excitation was not reported

in PES studies [19,23,43]. However, the 12.542 and 12.887 eV peaks in the HeI PES, which were assigned by Gochel-Dupuis et al. [43] as 3_0^2 (or 6_0^2 , see later) and 2_0^2 , respectively, can be re-assigned as 1_0^1 and 1_0^2 , respectively, giving a value $\nu_1 = 341$ meV in the ion ground state. Another possible PES assignment involving mode 1 is the 12.780 eV peak, assigned to $2_0^2 8_0^2$ by Gochel-Dupuis et al. [43], which can be re-assigned as $1_0^1 2_0^1$. The bands that we have reinterpreted were insufficiently resolved in PES spectra earlier than the high resolution study of Gochel-Dupuis et al. [43]. The value $\nu_1 = 341$ meV is in between those of the mode 1 frequency in the $2e \rightarrow 3e$ (328 meV) and the $2e \rightarrow 8a_1$ (353 meV) valence transition excited states, from which we can conclude that the 3e (and $8a_1$) orbitals are fairly neutral with respect to C–H bonding, thus confirming the interpretation preferred above. We remark that in the 2^2E state of the ion, formed by removal of a 1e electron, the drop to $\nu_1 = 345$ meV is similar to that in 1^2E , being only 6%, which indicates that 1e, too, is CH bonding, to about the same extent as 2e, and not antibonding as previously proposed [19].

4.4.2. Mode 2

The C≡N stretching mode 2 decreases in frequency by 15% in the two $2e \rightarrow 3e$ excitation transitions, 20% when 2e is promoted to $8a_1$, and 15% in $7a_1 \rightarrow 8a_1$. This indicates that 2e and $7a_1$ are CN bonding and that $7a_1$, which is classified as a σ_{CN} orbital, is less CN bonding than 2e. In the ground state of the acetonitrile ion, formed by removing one 2e electron, $\nu_2 = 246$ meV, a comparable decrease to that in the $2e \rightarrow 3e$ excitation. We note also that in the 2^2E state of the ion the 6% decrease in ν_2 suggests that 1e is also CN bonding, but less so than 2e.

4.4.3. Mode 3

In He photoelectron spectra, the vibration of frequency 171 meV in the ion ground state has been assigned as being either the CH_3 sym-deformation mode 3 or as the CH_3 antisymmetric deformation mode 6 [43], which have similar frequencies in the neutral ground state. However, mode 3 drops by about 25% in the 1^1E , 3^1A_1 and 2^1E states, which is consistent with 2e being CH bonding, as discussed above. We are thus led to propose that the 171 meV frequency be assigned to mode 6 in the 1^2E state of the ion. Loss of a $7a_1$ electron does not affect very much the CH_3 deformation modes 3 and 6 in the 1^2A_1 ion state (Table 5). The frequency of 182 meV in the 2^2E ion state was assigned by Gochel-Dupuis et al. [43] to mode 3, which would represent an increase of about 6% in the $1e^{-1} 2^2E$ state. Since its frequency is close to that of mode 6 in the neutral ground state, 180 meV, we suggest that it could very well also be assigned to mode 6 in the 2^2E state of the ion, or to both, unresolved, modes 3 and 6.

4.4.4. Mode 4

Mode 4 is the carbon–carbon stretching mode. It has a frequency of 101 meV in the $2e^{-1} 1^2E$ ion state, a decrease

Table 5
Vibrational frequencies in meV of acetonitrile valence and ion states

	Mode							
	1	2	3	4	5	6	7	8
State 1^1A_1	366	281	172	114	373	180	129	45
$1^1E(I)^b$	353	224	126	90				
$2^1E(II)$	328	239	133	90				
$2^1A_1(III)$		264		101				69
$3^1A_1(IV)$	334	245	126	98				
$1^2E(\text{ion})$	341	246		101		171 ^a		50
$1^2A_1(\text{ion})$			162	100 ^a		180		50
$2^2E(\text{ion})$	345	259	182	103				

^a Ion state frequencies from [43] and see text.

^b Valence transitions: I = $1^1E \leftarrow 1^1A_1$, $2e \rightarrow 8a_1$, $\pi \rightarrow \sigma^*$; II = $2^1E \leftarrow 1^1A_1$, $2e \rightarrow 3e$, $\pi \rightarrow \pi^*$; III = $2^1A_1 \leftarrow 1^1A_1$, $7a_1 \rightarrow 8a_1$, $n \rightarrow \sigma^*$; IV = $3^1A_1 \leftarrow 1^1A_1$, $2e \rightarrow 3e$, $\pi \rightarrow \pi^*$.

of 14% from the neutral ground state, showing that the 2e M.O. is C–C bonding. We have discussed above our reasons for re-assigning as 4_0^n the bands that Eden et al. [35] assigned to 8_0^n transitions. Mode 4 is excited in the $2e \rightarrow 3e$ valence transitions II and IV and also in the $2e \rightarrow 8a_1$ transition I, with a frequency of 90 meV in both 1^1E and 2^1E states, a decrease of 21% with respect to the 1^1A_1 state, and with a frequency of 96 meV in the 3^1A_1 state and 101 meV in the $7a_1 \rightarrow 8a_1$ 2^1A_1 state. We conclude that the 3e and $8a_1$ M.O.s are C–C antibonding and that the $7a_1$ orbital is less C–C bonding than 2e. The vibrational frequencies in the first excited state 1^2A_1 of the ion, observed by high resolution photoelectron spectroscopy were given tentative assignments involving ν_8 [43]. It is possible to reinterpret the spectrum to extract a value for the mode 4 frequency, $\nu_4 = 100$ meV, close to the value in valence state 2^1A_1 where a $7a_1$ electron has been promoted (Table 5). The $1e^{-1} 2^2E$ ion state has $\nu_4 = 103$ meV, which suggests that 1e is C–C bonding to about the same extent as 2e.

4.5. Rydberg transitions

Fig. 3 shows our absorption spectrum in the 9–13.5 eV range. It is better resolved than that of Nuth and Glicker [38] in the same energy region, as well as the electron energy loss spectrum of Gochel-Dupuis et al. [34]. It is also better resolved than the spectrum of Eden et al. [35], and slightly better than that of Suto and Lee [42], in the respective common energy regions. Our measured peak energies (Table 6) are generally in good agreement (to within less than 10 meV) with those reported by Nuth and Glicker [38] (absorption 9.595–13.099 eV) and by Gochel-Dupuis et al. [34] (EELS 9.589–11.947 eV), and to within 5 meV with those of Eden et al. [35] (absorption 8.93–10.772 eV).

Our measurements include a few previously unresolved peaks as new data. In cases where we have observed features previously unreported in the publications of Gochel-Dupuis et al. [34] and of Eden et al. [35] we have measured their published spectra to see if these features are also present (Table 6). The detailed vibronic analyses of Nuth and Glicker (optical absorption) and of Gochel-Dupuis et al. (EELS) of Rydberg series converging to the ion ground state 1^2E and first excited state 1^2A_1 have been added to, in part, by Eden et al. (absorption). Their assignments are given in Table 6. Assignments of Rydberg transitions converging to the first excited electronic state 1^2A_1 of the ion are distinguished from those leading to the 1^2E ground state by being in italics. We have significantly revised previous Rydberg series assignments, especially of the Rydberg bands converging to the first excited state of the ion, essentially as a result of observing a very clear set of bands in particular above 12.2 eV which converge to the 1^2A_1 state of the ion, with a quantum defect $\delta \approx 1$ (see below).

4.5.1. Rydberg series converging to the ion ground state 1^2E

We first discuss Rydberg bands converging to the ground state of the ion. Gochel-Dupuis et al. [34] did not report any members of the $n\sigma$ series. Only one member of this series, the 3σ O_0^0 band at 8.926 eV (our measurement value), was assigned by Eden et al. [35] and by Nuth and Glicker [38]. However, Nuth and Glicker assigned also the $n = 4-9$ members. We carefully examined the EELS spectra of Gochel-Dupuis et al. to see if $n \geq 3$ Rydbergs were present but not reported. Features that we found were present are indicated in parentheses in Table 6, or as P if precise energy measurement was not possible because of band shape or weakness. These include the $n = 4-6$ members that Nuth and Glicker [38] reported at 10.744,

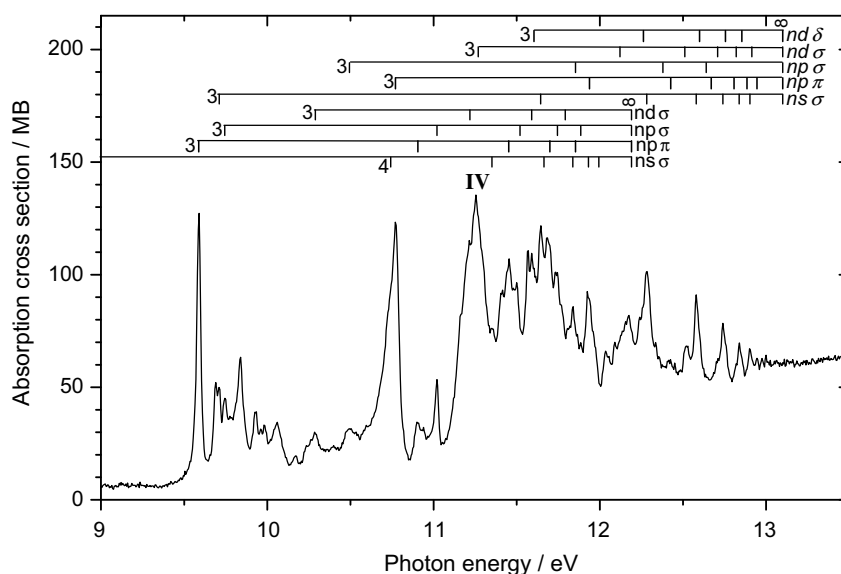


Fig. 3. Absorption spectrum of acetonitrile in the range 9–13.5 eV. IV indicates the O_0^0 origin band of the valence transition $3^1A_1 \leftarrow 1^1A_1$.

Table 6
Acetonitrile absorption peak energies (eV): Rydberg series^{a,b}

Present study	Nuth and Glicker [38]	Gochel-Dupuis et al. [34] ^c	Eden et al. [36] ^d
8.926 3sσO ₀ ⁰	8.930 3sσO ₀ ⁰		8.93 3sσO ₀ ⁰
9.588 3pπO ₀ ⁰	9.595 3pσO ₀ ⁰	9.589 3pπO ₀ ⁰	9.589 3pπO ₀ ⁰
	9.678 3pπO ₀ ⁰		
9.689 3pπ4 ₀ ¹	9.695 3pσ4 ₀ ¹	9.694 3pπ4 ₀ ¹	9.694 3pπ4 ₀ ¹
9.711 3sσO ₀ ⁰ ; 3pπ3 ₀ ¹	9.716 3pσO ₀ ⁰	(9.720)	9.709 unassigned
9.744 3pσO ₀ ⁰		9.745 3pσO ₀ ⁰	9.747 3pσO ₀ ⁰
9.781 3pπ4 ₀ ²		P	9.786 unassigned
9.811 3pπ3 ₀ ¹ 4 ₀ ¹		(9.811)	(9.810)
9.837 3pπ2 ₀ ¹ ; 3pπ3 ₀ ²	9.842 3pσ2 ₀ ¹	9.838 3pπ2 ₀ ¹	9.840 3pπ2 ₀ ¹
9.866 3pσ3 ₀ ¹			(9.861)
9.912 3pπ3 ₀ ¹ 4 ₀ ²			
9.931 3pπ2 ₀ ¹ 4 ₀ ¹ ; 3pπ1 ₀ ¹	9.935 3pσ2 ₀ ¹ 4 ₀ ¹	9.929 3pπ2 ₀ ¹ 4 ₀ ¹	9.935 3pπ2 ₀ ¹ 4 ₀ ¹
9.961 3pπ3 ₀ ¹		P	(9.959)
9.982 3pσ2 ₀ ¹	9.983 3pπ2 ₀ ¹	9.973 3pσ2 ₀ ¹	9.983 3pσ2 ₀ ¹
10.034 3pπ1 ₀ ¹ 4 ₀ ¹		(10.031)	(10.024)
10.058 3pπ2 ₀ ² ; 3pπ1 ₀ ³	10.056 3pσ2 ₀ ²	10.060 3pπ2 ₀ ²	10.064 3pπ2 ₀ ²
10.171 3pπ2 ₀ ² 4 ₀ ¹	10.181 3pσ2 ₀ ² 4 ₀ ¹	10.182 3pπ2 ₀ ² 4 ₀ ¹	10.171 3pπ2 ₀ ² 4 ₀ ¹
10.234 3pσ2 ₀ ²		(10.222)	10.250 3pσ2 ₀ ²
10.262 3pπ1 ₀ ²		(10.263)	(10.264)
10.289 3dσO ₀ ⁰	10.292 3dσO ₀ ⁰	10.286 3dσO ₀ ⁰	10.289 3dσO ₀ ⁰
10.400 3dσ4 ₀ ¹		10.415 3dσ4 ₀ ¹	10.401 3dσ4 ₀ ¹
10.494 3pσO ₀ ⁰	10.501 3dσ2 ₀ ¹	(10.484)	10.489 3pσO ₀ ⁰
		10.520 3pσO ₀ ⁰	
10.527 3dσ2 ₀ ¹		10.531 3dσ2 ₀ ¹	10.53 3dσ2 ₀ ¹
10.596 3pπ1 ₀ ³ ; 3pσ4 ₀ ¹		(10.600)	10.59 3pσ4 ₀ ¹
10.632 3dσ1 ₀ ¹		(10.628)	10.64 3dσ2 ₀ ¹ 4 ₀ ¹
10.687 3pσ2 ₀ ¹		(10.686)	10.70 3pσ2 ₀ ¹
10.742 4sσO ₀ ⁰	10.744 4sσO ₀ ⁰	(10.743)	10.74 3dσ2 ₀ ²
10.771 3pπO ₀ ⁰ ; 3dσ2 ₀ ²	10.778 3pπO ₀ ⁰	10.780 3pλO ₀ ⁰	10.772 3pλO ₀ ⁰
10.906 4pπO ₀ ⁰	10.918 4pσO ₀ ⁰	10.916 4pπO ₀ ⁰	
10.940 3pπ3 ₀ ¹	10.941 3pπ3 ₀ ¹	10.937 3pλ3 ₀ ¹	
10.984 4sσ2 ₀ ¹	11.007 4pπO ₀ ⁰	(11.0)	
11.020 4pσO ₀ ⁰	11.027 4pσ4 ₀ ¹	11.029 4pσO ₀ ⁰	
11.089 4sσ2 ₀ ¹ 4 ₀ ¹			
11.122 4pσ4 ₀ ¹			
11.165 4pπ2 ₀ ¹	11.177 4pσ2 ₀ ¹	(11.175)	
11.218 4dσO ₀ ⁰	11.221 4dσO ₀ ⁰	11.220 4dσO ₀ ⁰	
11.239 4pπ1 ₀ ¹			
11.256 4pσ2 ₀ ¹	11.266 4pσ2 ₀ ¹ 4 ₀ ¹		
3¹A₁ ← 1¹A₁O₀⁰			
11.269 3dσO ₀ ⁰		11.268 3dσO ₀ ⁰	
11.292 4pπ2 ₀ ¹ 3 ₀ ¹	11.307 4pπ2 ₀ ¹	(11.328)	
11.351 5sσO ₀ ⁰ ; 3dσ4 ₀ ¹	11.345 5sσO ₀ ⁰	(11.344)	
3¹A₁ ← 1¹A₁4₀¹			
11.382 3 ¹ A ₁ ← 1 ¹ A ₁ 3 ₀ ¹	11.361 3dσO ₀ ⁰	(11.363)	
11.418 3dσ3 ₀ ¹	11.374 4pσ2 ₀ ²		
11.452 5pπO ₀ ⁰ ; 3dσ4 ₀ ²	11.416 4dσ2 ₀ ¹	11.422 3dσ3 ₀ ¹	
	11.465 5pσO ₀ ⁰	11.467 5pπO ₀ ⁰	
3¹A₁ ← 1¹A₁4₀²			
11.500 3dπO ₀ ⁰ ; 4pσ2 ₀ ²	11.491 4pσ2 ₀ ² 4 ₀ ¹	11.503 3dπO ₀ ⁰	
3¹A₁ ← 1¹A₁2₀¹			
11.520 5pσO ₀ ⁰	11.512 5pπO ₀ ⁰	11.516 5pσO ₀ ⁰	
11.567 5pπ4 ₀ ¹ ; 3dσ3 ₀ ²	11.578 5pσ4 ₀ ¹		
11.590 5dσO ₀ ⁰	11.590 5dσO ₀ ⁰	11.587 5dσO ₀ ⁰	
3¹A₁ ← 1¹A₁1₀¹			
11.604 3dδO ₀ ⁰	11.607 4pσO ₀ ⁰	11.602 3dδO ₀ ⁰	
11.644 4sσO ₀ ⁰			
11.664 6sσO ₀ ⁰	11.666 6sσO ₀ ⁰	11.662 3dπ3 ₀ ¹	
11.682 5dσ4 ₀ ¹		(11.683)	
11.700 6pπO ₀ ⁰	11.701 5pσ2 ₀ ¹	11.704 6pπO ₀ ⁰	

(continued on next page)

Table 6 (continued)

Present study	Nuth and Glicker [38]	Gochel-Dupuis et al. [34] ^c	Eden et al. [36] ^d
11.745 $6p\sigma O_0^0$;	11.717 $6p\sigma O_0^0$ 11.745 $6p\pi O_0^0$	P	
$3^1A_1 \leftarrow 1^1A_1 2_0^2$			
11.769 $3d\delta 3_0^1$	11.765 $4p\sigma 3_0^1$	11.759 $3d\delta 3_0^1$	
11.792 $6d\sigma O_0^0$	11.786 $6d\sigma O_0^0$	(11.774)	
11.799 $5p\pi 1_0^1$	11.797 $5d\sigma 2_0^1$	(11.796)	
	11.801 $5p\sigma 2_0^1 4_0^1$	(11.804)	
11.805 $6p\pi 4_0^1$	11.808 $5p\pi 2_0^1$		
11.820 $6p\pi 4_0^1$; $6s\sigma 3_0^1$	11.819 $6p\sigma 4_0^1$		
11.837 $7s\sigma O_0^0$	11.828 $7s\sigma O_0^0$		
11.854 $7p\pi O_0^0$; $4p\sigma O_0^0$	11.849 $7p\sigma O_0^0$	11.849 $4p\sigma O_0^0$	
11.885 $7p\sigma O_0^0$	11.876 $7p\pi O_0^0$		
	11.903 $7d\sigma O_0^0$		
	11.926 $5p\sigma 2_0^2$	(11.929)	
11.932 $8s\sigma O_0^0$	11.935 $8s\sigma O_0^0$		
11.938 $4p\pi O_0^0$	11.940 $4p\pi O_0^0$	11.947 $4p\lambda O_0^0$	
11.956 $8p\sigma O_0^0$; $4p\sigma 4_0^1$	11.952 $6p\sigma 2_0^1$; $8p\sigma O_0^0$		
11.975 $7s\sigma 3_0^1$	11.975 $7p\sigma 4_0^1$		
	11.992 $6d\sigma 2_0^1$		
11.994 $9s\sigma O_0^0$;	11.997 $9s\sigma O_0^0$		
$3^1A_1 \leftarrow 1^1A_1 2_0^3$			
12.016 $4p\sigma 3_0^1$	12.011 $9p\sigma O_0^0$		
12.035 $8s\sigma 4_0^1$; $4p\pi 4_0^1$	12.015 $9p\pi O_0^0$		
	12.032 $6p\pi 2_0^1$		
12.054 $8p\pi 4_0^1$; $4p\sigma 4_0^2$	12.036 $5p\sigma 2_0^1 4_0^1$		
12.091 $4p\pi 3_0^1$	12.064 $6p\sigma 2_0^1 4_0^1$		
12.114 $4p\sigma 3_0^1 4_0^1$	12.107 $4p\pi 3_0^1$		
12.121 $4d\sigma O_0^0$	12.111 $7p\sigma 2_0^1$		
12.132 $6d\sigma 1_0^1$; $7p\pi 2_0^1$; $8s\sigma$	12.119 $7d\sigma 2_0^1$		
4_0^2 ; $4p\pi 4_0^2$			
12.156 $4p\sigma 4_0^3$	12.169 $7p\pi 2_0^1$		
12.173 $4p\sigma 3_0^1$	12.176 $4d\sigma O_0^0$		
12.186 $8p\pi 2_0^1$	12.190 $6p\sigma 2_0^2$		
	12.204 $7p\sigma 2_0^1 4_0^1$		
12.240 $4d\pi O_0^0$; $4p\sigma 3_0^2 4_0^1$			
12.262 $4d\delta O_0^0$; $4p\sigma 4_0^4$			
12.282 $5s\sigma O_0^0$	12.296 $5p\sigma O_0^0$		
	12.304 $6p\sigma 2_0^2 4_0^1$		
12.335 $4d\sigma 4_0^1$	12.333 $7p\sigma 2_0^2$		
12.355 $4d\delta 4_0^1$			
12.379 $5p\sigma O_0^0$; $5s\sigma 4_0^1$			
12.411 $4d\pi 3_0^1$			
12.426 $5p\pi O_0^0$			
12.450 $5s\sigma 3_0^1$	12.440 $5p\pi O_0^0$		
12.482 $5s\sigma 4_0^2$	12.447 $7p\sigma 2_0^2 4_0^1$		
12.511 $5d\sigma O_0^0$	12.462 $5p\sigma 3_0^1$		
12.528 $5p\pi 4_0^1$			
12.580 $6s\sigma O_0^0$	12.526 $5d\sigma O_0^0$		
12.600 $5d\delta O_0^0$	12.598 $6p\sigma O_0^0$		
12.623 $5p\pi 4_0^2$			
12.640 $6p\sigma O_0^0$	12.621 $5p\pi 3_0^1$		
12.670 $6p\pi O_0^0$			
12.684 $6s\sigma 4_0^1$	12.667 $6p\pi O_0^0$		
12.708 $6d\sigma O_0^0$			
12.740 $7s\sigma O_0^0$; $6s\sigma 3_0^1$;	12.701 $6d\sigma O_0^0$		
$6p\sigma 4_0^1$			
12.756 $6d\delta O_0^0$; $5d\delta 3_0^1$	12.756 $7p\sigma O_0^0$		
12.788 $6s\sigma 4_0^1$	12.761 $6p\sigma 3_0^1$		
12.807 $7p\pi O_0^0$	12.806 $7p\pi O_0^0$		

Table 6 (continued)

Present study	Nuth and Glicker [38]	Gochel-Dupuis et al. [34] ^c	Eden et al. [36] ^d
12.820 $7d\sigma O_0^0$			
12.838 $8s\sigma O_0^0$; $7p\sigma 4_0^1$	12.838 $7d\sigma O_0^0$		
	12.846 $6p\pi 3_0^1$		
12.854 $7d\delta O_0^0$	12.856 $8p\sigma O_0^0$		
12.885 $8p\pi O_0^0$	12.883 $8p\pi O_0^0$		
12.903 $9s\sigma O_0^0$; $7p\pi 4_0^1$	12.904 $8d\sigma O_0^0$		
12.914 $8d\sigma O_0^0$	12.912 $9p\sigma O_0^0$		
	12.923 $7p\sigma 3_0^1$		
12.945 $9p\pi O_0^0$	12.938 $9p\pi O_0^0$		
	12.954 $9d\sigma O_0^0$		
12.976 $7p\pi 3_0^1$	12.962 $7p\pi 3_0^1$		
12.999 $9s\sigma 4_0^1$			
13.010 $7d\delta 3_0^1$	13.020 $8p\sigma 3_0^1$		
13.034			
13.048 $8p\pi 3_0^1$; $9p\pi 4_0^1$	13.050 $8p\pi 3_0^1$		
13.061 $9s\sigma 3_0^1$			
13.081 $8d\sigma 3_0^1$	13.081 $9p\sigma 3_0^1$		
13.097 $9p\pi 3_0^1$	13.099 $9p\pi 3_0^1$		
13.116			
14.212 ^e			
14.298			
14.390			
14.490			
14.537			
14.695			
14.813			
14.878			
14.994			
15.110			
15.163			
15.181			
15.332			

^a Note that $ns\sigma = nsa_1$, $np\sigma = npa_1$, $np\pi = npe$, $nd\sigma = nda_1$, $nd\pi = nde(1)$, $nd\delta = nde(2)$ in going from axial model (pseudo-diatomic) to C_{3v} .

^b $3^1A_1 \leftarrow 1^1A_1$ valence transition bands in bold.

^c Gochel-Dupuis et al. [34]: in parentheses non-reported weak features that we have measured from their Figs. 3 and 4. P = non-reported weak feature present in their Figs. 3 or 4 at about our corresponding peak energies but precise measurement not possible because of band shape or weakness.

^d Eden et al. [36], in parentheses non-reported weak features that we have measured from their Fig. 8.

^e See text for possible assignments of features ≥ 14.212 eV.

11.345 and 11.666 eV. In the spectra of Eden et al. [35], whose upper limit is 10.8 eV, there is a band at 10.74 eV, assigned by them as $3d\sigma 2_0^2$. In our analysis the latter occurs at 10.771 eV, giving a correct value for the mode 2 vibrational frequency (see later). Within the 12 eV upper limit of the EELS spectra of Gochel-Dupuis et al. there is no sign, at their resolution, of features that could be attributed to the $n = 7$ and 8 members of the $ns\sigma$ series. Our assignments for this series are the same as those of Nuth and Glicker. One small difference with Gochel-Dupuis et al. concerns the $6s\sigma O_0^0$ band, which we observe at 11.664 eV (given as 11.666 eV by Nuth and Glicker) but the band reported by Gochel et al. at 11.662 eV is assigned by them to $3d\pi 3_0^1$. Although the scale of the published spectrum (Fig. 4 of Nuth and Glicker [38]) is insufficient for its exact measurement, we suggest that 11.668/2 eV corresponds to an unresolved pair of bands in their spectra but resolved in ours and which we report at 11.644 eV ($4s\sigma O_0^0$) and 11.682 eV ($5d\sigma 4_0^1$). The average quantum defect for the O_0^0 bands of the $ns\sigma$ series is $\delta = 0.93$. Vibrational

components of the various Rydberg series are discussed later (Section 4.5.2).

The intense band at 9.588 eV has been assigned as $3p\sigma O_0^0$ by Nuth and Glicker [38] and $3p\pi O_0^0$ by Gochel-Dupuis et al. [34] and by Eden et al. [35]. This raises the question concerning the relative order of the npe and npa_1 Rydberg levels. Fridh [33] considers that $np\sigma$ levels (here npa_1 in C_{3v} symmetry) lie below the $np\pi$ (npe in C_{3v}), in accordance with an expectation that the quantum defect of a $np\sigma$ level should be greater than of the corresponding $np\pi$ level, following an electrostatic approach and with the reasoning of Lindholm [44]. However, on the basis of the existence of a slight minimum in the 20 and 70 eV elastic scattering differential cross sections for the $3p\sigma$ state feature at 9.589 eV, Gochel-Dupuis et al. [34] argue in favour of excitation of a $2e \rightarrow 3pe$ Rydberg transition, thus suggesting that the $3pa_1$ ($3p\sigma$) level lies above the $3pe$ ($3p\pi$) level. This Rydberg level order was adopted by Gochel-Dupuis et al. and, without discussion, by Eden et al. The question of the relative order of the

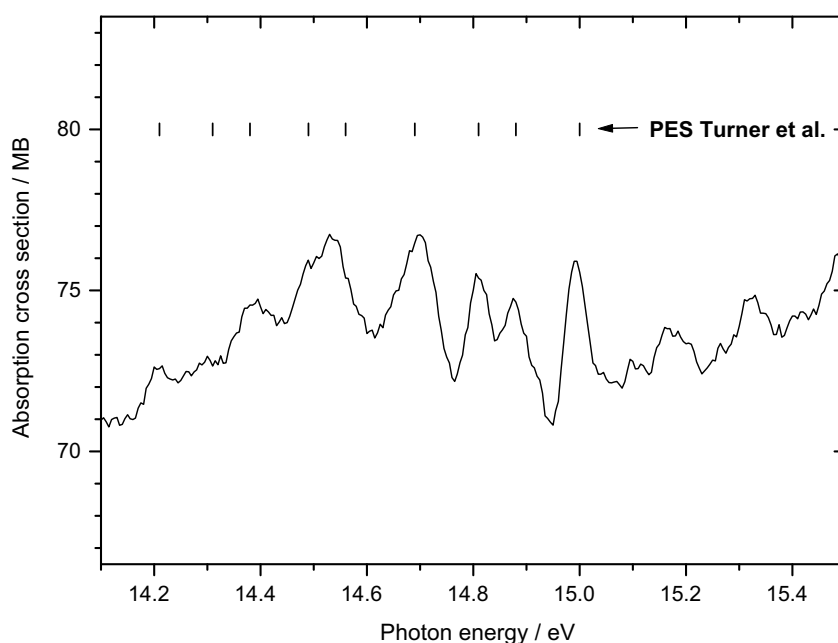


Fig. 4. Comparison between acetonitrile absorption features in the 14.1–15.5 eV region and, as vertical bars, the energies, diminished by 0.92 eV, of the vibronic features of the third photoelectron band in the HeI photoelectron spectrum [19], between 15.1 and 16 eV.

$3p\pi$ and $3p\sigma$ levels also arises in the interpretation of fluorescence excitation spectra of acetonitrile [12].

If the $n\rho\sigma$ levels lie above the $n\rho\pi$ it follows that the quantum defects of the $p\pi$ states will then be bigger than those of corresponding $p\sigma$ states. Such level order and associated quantum defect behaviour exists for open shell molecules such as O_2 and NO but relatively rarely for closed shell molecules [44], and is not expected, in particular, for linear systems [45]. Indeed, calculations predict $n\rho\sigma$ levels to lie below $n\rho\pi$ in a large number of molecules, including both planar and nonplanar species [45]. Acetonitrile is a closed shell molecule, isoelectronic with CO_2 and N_2O , both of which have the $n\rho\sigma$ levels below the $n\rho\pi$, so it is reasonable to expect the same Rydberg level order behaviour in the latter. Nevertheless, in our own assignments in Table 6 we have provisionally adopted the orbital order $n\rho\pi$ as lying below $n\rho\sigma$. However, as stated above, this order assignment of Gochel-Dupuis et al. [34] is based on the observation of a slight minimum in the elastic scattering differential cross sections, but this minimum is due to a single point in their measurements. Their conclusion needs to be firmly established so that measurements of elastic scattering differential cross sections at smaller angle intervals are necessary to clarify these observations and interpretations.

Our assignments of the $n\rho\pi$ series ($n = 3-7$) is identical to that of Gochel-Dupuis et al. [34]. The average quantum defect for the O_0^0 bands of the $n\rho\pi$ series is $\delta = 0.75$. The $n\rho\sigma$ assignments for $n = 3-5$ are also the same as those of Gochel-Dupuis et al. and we extend this series to $n = 7$ and 8. The O_0^0 band quantum defect average for this series is $\delta = 0.55$.

In addition to $n\rho\sigma$ and $n\rho\pi$ transitions, we have also assigned $nd\sigma$ Rydbergs ($n = 3-6$), confirming the previous

assignments of Nuth and Glicker [38] and of Gochel-Dupuis et al. [34] (Table 6). The average quantum defect for the O_0^0 bands of the $nd\sigma$ series is $\delta = 0.28$. For these three series of Rydberg transitions converging to the ion ground state, the reported quantum defects [34,35,38] determined on the basis of the various assignments are all reasonable, even though some differences exist concerning the bands that are assigned to higher members of the $n\rho\sigma$, $n\rho\pi$ and $nd\sigma$ transitions in the analyses of Nuth and Glicker [38] and of Gochel-Dupuis et al. [34] (Table 6). The assignments of Eden et al. [35] are mostly identical with those of Gochel-Dupuis et al. Our average quantum defects for the O_0^0 bands of Rydberg transitions converging to the ground and first excited state of the ion are given in Table 7. In this table they are compared with the values which we have calculated from the published peak energies of Gochel-Dupuis et al. [34], Rianda et al. [36] and Fridh [33], using 12.201 eV and 13.131 eV as the values of the ionization energies of the ground and first excited state of the acetonitrile ion. Note that our peak energy resolution is certainly better than in the EELS measurements [33,34,36] especially in those of Rianda et al. [36].

4.5.2. Rydberg series converging to the ion first excited state 1^2A_1

The assignments of Nuth and Glicker [38] of transitions converging to the first excited state 1^2A_1 of the ion include $ns\sigma$, $n\rho\sigma$, $n\rho\pi$ and $nd\sigma$ Rydbergs. These authors assign $3s\sigma$ to lie below $3p\pi$, as they did for the corresponding Rydberg levels converging to the 1^2E ground state. Gochel-Dupuis et al. [34] consider that their differential cross section data as being compatible with bands being either $n\rho\sigma$ or $n\rho\pi$ and they apparently remain neutral on this question by labelling bands as $n\rho\lambda$ although there is some ambiguity on this

Table 7
Quantum defects: average values for O_0^0 bands

Rydberg series	Present study	Gochel-Dupuis et al. [34]	Rianda et al. [36]	Fridh [33]
$ns\sigma$	0.93 ($n = 3-9$)	0.98 ($n = 3$) ^a		0.96 ($n = 3, 4$)
$np\pi$	0.75 ($n = 3-7$)	0.73 ($n = 3-6$)	0.72 ($n = 3, 4$) ^b	0.74 ($n = 3, 4$) ^b
$np\sigma$	0.55 ($n = 3-8$)	0.59 ($n = 3-5$)		0.60 ($n = 4$) ^c
$nd\sigma$	0.28 ($n = 3-6$)	0.30 ($n = 3-5$)	0.28 ($n = 3, 4$)	0.31 ($n = 3, 4$)
1^2E ion state limit 12.201 eV				
$ns\sigma$	1.02 ($n = 3-7$) ^d			0.98 ($n = 4-9$) ^e
$np\pi$	0.59 ($n = 3-9$)	0.60 ($n = 3, 4$)	0.61 ($n = 3$)	0.59 ($n = 3-5$)
$np\sigma$	0.74 ($n = 3-6$)	0.73 ($n = 3, 4$)	0.67 ($n = 3, 4$)	
$nd\sigma$	0.31 ($n = 3-8$)	0.30 ($n = 3$)	0.30 ($n = 3, 4$)	0.26 ($n = 3-5$)
$nd\pi$	0.10 ($n = 3, 4$)	0.11 ($n = 3$)	0.08 ($n = 3-7$) ^f	
$nd\delta$	0.02 ($n = 3-7$)	0.02 ($n = 3$)		
1^2A_1 ion state limit 13.131 eV				

^a Eden et al. data [36].

^b Assigned as $np\sigma$ [33,36].

^c Assigned as $np\pi$ [33].

^d Assigned $n = 3-9$.

^e Assigned as $np\sigma$ [33].

^f See text.

matter since, in the same paper, they make a definite assignment of $3p\sigma$ and $4p\sigma$ at 10.520 and 11.849 eV, respectively, in agreement with Rianda et al. [36]. This implies that the bands at 10.780 and 11.940 eV, assigned as $3p\lambda$ and $4p\lambda$, are $3p\pi$ and $4p\pi$. The $np\lambda$ nomenclature and the $3p\sigma$, $4p\sigma$ assignments are followed by Eden et al. [35] for Rydbergs converging to the 1^2A_1 state of the ion.

Gochel-Dupuis et al. [34], following Nuth and Glicker [38], did not assign any members of the $ns\sigma$ series. Our observations of strong features beyond 12 eV, forming obvious Rydberg series with a quantum defect close to unity enabled us to assign the $n = 3-10$ members of the $ns\sigma$ series (Fig. 3). A set of bands at similar or close-lying peak energies were observed and assigned by Nuth and Glicker, as well as by Fridh [33], to the $np\sigma$ series, although Fridh considers that an alternative assignment to $ns\sigma$ can also be envisaged, depending on whether the analogous transitions can be found in HCN. Indeed, the more recent high resolution absorption spectral observation and assignment of both $ns\sigma$ and $np\sigma$ series in HCN [38], whose respective quantum defects are $\delta = 0.99$ and $\delta = 0.66$, supports our assignment of the $ns\sigma$ series in acetonitrile.

In our interpretation, the $np\sigma$ series has four members ($n = 3-6$), with an average $\delta = 0.74$ (Table 7). The first member of this series was assigned by Gochel-Dupuis et al. [34] to a band at 10.520 eV, mentioned previously, which was not observed by us or by other authors [33,35,38]. Our assigned $3p\sigma$ band at 10.494 eV was observed at 10.489 eV and assigned as $3p\sigma$ by Eden et al, and this undoubtedly corresponds to the band at 10.484 eV in the spectrum of Gochel-Dupuis et al. [34], at 10.496 eV in the EELS of Fridh [33], and at 10.501 eV in the absorption spectrum of Nuth and Glicker [38] (Table 6).

The $np\pi$ series has seven members ($n = 3-9$), with average $\delta = 0.59$, the first two of which were also observed and assigned by Eden et al. and by Gochel-Dupuis et al. [34].

Nuth and Glicker [38] assign the same seven members of this series ($n = 3-9$) (Table 6).

The six members of the $nd\sigma$ series ($n = 3-8$) have an average quantum defect $\delta = 0.31$. A value of this order of magnitude for the $nd\sigma$ series is reasonable for a polyatomic molecule such as acetonitrile [44]. Bands of this series were assigned by Nuth and Glicker [38], mainly to features other than those we assigned to $nd\sigma$. In our analysis of the absorption spectrum, the first member of this series, at 11.269 eV is close to the most intense band in the spectrum which is at 11.256 eV (Fig. 3). We recall that our calculations predict several high energy allowed valence transitions (Table 2) and that HAM/3 calculations [33] predict a $2e \rightarrow 3e$ transition to the 3^1A_1 state at 11.9 eV, (calculated by us to have $f \approx 0.1$), and a $1e \rightarrow 3e$ transition to an allowed 1^1A_1 state at 12.4 eV. Indeed, Fridh assigned the 11.256 eV band to the $3^1A_1 \leftarrow 1^1A_1$ valence transition [33]. We follow this assignment and propose that this band as the O_0^0 feature and that vibrational components of the $3^1A_1 \leftarrow 1^1A_1$ transition involving excitation of modes 1-4 (Table 5) overlap with some of the Rydberg bands (Table 6).

Two other nd series were observed, the $nd\pi$, with its two members $n = 3$ and 4, average $\delta = 0.10$, and the more extensive $nd\delta$, for which we observed the five members $n = 3-7$, whose average $\delta = 0.02$. The $n = 3$ members of both series were observed by Gochel-Dupuis et al. [34]. Rianda et al. [36] reported the same five members of the $nd\pi$ series ($n = 3-7$), at EELS peak energies compatible with our better resolved absorption spectrum.

We note that vibronic absorption peaks between 12.28 and 13 eV, and which correspond to Rydberg series converging to the first excited electronic state of the cation, are also observed in the parent ion yield curve [46]. These features also occur in the CN(A-X) and CN(B-X) fluorescence excitation spectra, as discussed elsewhere [12].

Table 6 contains a number of our re-assignments of previously observed bands. In particular we assign Rydberg bands in which vibrational modes 1 and 3 are excited. The vibrational frequencies derived from previous Rydberg band analyses [33–35,38] and from our re-assignments are consistent with the values derived for the ion states from photoelectron spectroscopy (PES) studies [43], including our suggested re-assignments of the PES discussed above. The Rydberg levels which converge to the ion ground state 1^2E have as associated vibrational frequencies $\nu_1 = 343$ meV (ion 341 meV, see above), $\nu_2 = 249$ and 238 (ion 246) meV, $\nu_4 = 101$ (ion 101) meV. Rydberg bands which converge to the first excited state of the ion, 1^2A_1 have vibrational components whose frequencies are $\nu_3 = 162$, 156 and 157 (ion 162) meV, $\nu_4 = 101$ (ion 101) meV.

The very large number of absorption peaks at small energy intervals, in particular in the regions close to ionization limits, makes possible a variety of vibronic assignments without having conclusive checks on these assignments. After exhaustive examination of our absorption spectra, and comparison with relevant previous publications, we consider that validation of the extant analyses of both Rydberg and valence transitions calls for further studies with deuterated acetonitrile isotopologues, which we hope eventually to carry out.

4.6. Higher energy absorption region

In the region above 13 eV we observe clearly a set of absorption bands between 13.9 and 15.5 eV (Fig. 1) and some weak features, barely above the noise level, overlying a broad continuum between 15.13 and 20 eV. These bands were not reported by Nuth and Glicker [38] but can be seen as barely resolved weak features in the part of their Fig. 4 which gives the absorption spectrum between 60 and 100 nm. We interpret them as being Rydberg features which belong to series converging to the second excited state of the ion, 2^2E , whose vibrationless level is at 15.133 ± 0.002 eV [43]. The broad feature mentioned above initiates at this energy. This is confirmed by the good match between these absorption features and the most intense of the vibronic features of the third photoelectron band in the HeI photoelectron spectrum [19,43], between 15.1 and 16 eV, corresponding to the formation of the origin level of the second excited electronic state of the acetonitrile ion at 15.133 ± 0.002 eV and to its vibrational components (Fig. 4). The absorption features lie about 0.92 eV below the corresponding PES features. However, unless the energy calibration of the absorption spectrum is incorrect, this leads the 14.212 eV band to correspond to absorption to a 4d Rydberg level, with a quantum defect of 0.16 or a 5s level with $\delta = 1.16$. It is possible that the 4d levels are less predissociated than the corresponding 5s and 5p levels since the Rydberg electrons of the latter would penetrate towards the nucleus much more than 4d. Although there are possibly some weak CN 383 nm bands

in the fluorescence excitation (FEX) spectrum in the region 14.7–15 eV, changes in predissociation rates do not show up clearly in the FEX spectrum [12]. It is possible that competitive predissociation might involve formation of ground state rather than electronically excited fluorescing products.

We remark that bands at 14.534 eV, 14.7 eV and 14.811 eV could conceivably correspond to higher members of these Rydberg series, but the weakness and relatively poor resolution of the features in the 14–15.3 eV region make it difficult to propose definite transition assignments, including vibrational components, for these features. However, the good match (Fig. 4) between the absorption spectrum features in the 14.212–15.8 eV region and the vibronic features of the third band of the photoelectron spectra, (after subtraction of 0.92 eV from the PES band energies), suggests, from vibronic analysis of the PES [19,43], that modes 3 and 4 are the most prominently excited vibrations, as components of the 4d or 5s Rydberg state in this part of the absorption spectrum. Their frequencies are $\nu_3 \approx 180$ meV and $\nu_4 \approx 100$ meV as determined from the PES. The problem of band assignment in this energy region also arises in comparison of absorption and ion yield spectra [12].

Starting at the energy corresponding to the formation of the 2^2E electronic state of the ion (15.133 eV) there is a rise in the absorption cross section to maxima of 81.5 mB at 16 and 16.6 eV, and 79.5 mB at 17.1 eV, with slight shallow dips at 16.3 and 16.8 eV, followed by a slow decrease in cross section to a value of 63 mB at 20 eV. The absorption spectra of Nuth and Glicker [38], less well resolved than ours, has a small minimum at 16.5 eV, a slight maximum at 17.5 eV and a cross section of 54 mB at 20 eV (values estimated by us from their Fig. 4).

5. Conclusion

VUV absorption spectra and electron energy loss spectra of acetonitrile have previously been studied by several authors [33–42] but previous assignments of valence and Rydberg transitions have suffered from an over reliance on vibronic data obtained from relatively low resolved photoelectron spectra, an insufficient appreciation of vibronic symmetry rules in the valence transitions and a lack of pertinent molecular orbital calculations of valence transitions and oscillator strengths. Our study was carried out at high resolution using monochromatised Kr lamp radiation (7.5–9.9 eV) and synchrotron radiation (7–20 eV) as photon excitation sources. We have reinterpreted, or assigned for the first time the bands of four valence transitions in the 7.9–12 eV region, ($\pi-\sigma^* 1^1E-1^1A_1$), ($\pi-\pi^* 2^1E-1^1A_1$), ($n-\sigma^* 2^1A_1-1^1A_1$), ($\pi-\pi^* 3^1A_1-1^1A_1$), aided by M.O. calculations of transition energies and oscillator strengths. These assignments also required consideration of vibronic symmetry conditions in electronic transitions not previously discussed in the context of the interpretation of acetonitrile VUV absorption spectra. Considerable revision of

previously assigned Rydberg transitions converging to the ground and first excited states of the cation in the 8.9–13.2 region was also effected. The vibrational modes and frequencies in the valence and Rydberg states have been determined and their correlation with the bonding characteristics of the valence shell molecular orbitals have been discussed in detail. Features are also observed in the 14.2–15.4 eV higher energy region which probably correspond to Rydberg series converging to the second excited state 2^2E of the ion at 15.133 eV. The spectral and the absorption cross sections which we have measured over the spectral range studied are potentially of use in understanding specific photodissociation and photoionization processes in acetonitrile, including those involving the solar flux or interstellar radiation, as discussed in a publication on the VUV photophysics of acetonitrile [12].

Acknowledgements

We acknowledge support from the European Commission Programme “Access to Research Infrastructures” for providing access to the Berlin BESSY synchrotron under contract FMRX-CT-0126. We thank the CNRS Groupe de Recherche “GDR Exobiologie” (GDR 1877) for support of this work.

References

- [1] A. Brack (Ed.), *The Molecular Origins of Life*, Cambridge University Press, Cambridge, UK, 1998.
- [2] P.M. Solomon, K.B. Jefferts, A.A. Penzias, R.W. Wilson, *ApJ* 168 (1971) L107.
- [3] S.V. Kalenskii, V.G. Promislov, A.V. Alakoz, A. Winnberg, L.E.B. Johansson, *Astron. Astrophys.* 354 (2000) 1036.
- [4] E. Araya, P. Hofner, S. Kurtz, L. Bronfman, S. DeDeo, *Astrophys. J. Suppl. Ser.* 157 (2005) 279.
- [5] L.E. Snyder, D. Buhl, *ApJ* 163 (1971) L47.
- [6] W.B. Huebner, L.E. Snyder, D. Buhl, *Icarus* 23 (1974) 580.
- [7] M.F. A'Hearn, M.J.S. Belton, W.A. Delamere, J. Kissel, et al., *Science* 310 (2005) 258.
- [8] L.M. Lara, E. Lellouch, J.J. López-Moreno, R. Rodrigo, *J. Geophys. Res.* 101 (1996) 23261.
- [9] A. Marten, T. Hidayat, Y. Biraud, R. Moreno, *Icarus* 158 (2002) 532.
- [10] E. Arijis, D. Nevejans, J. Ingels, *Int. J. Mass Spectrom. Ion Proc.* 81 (1987) 15.
- [11] K.H. Becker, A. Ionescu, *Geophys. Res. Lett.* 9 (1982) 1349.
- [12] M. Schwell, H.W. Jochims, H. Baumgärtel, S. Leach, *Chem. Phys.* (2007), this issue, doi:10.1016/j.chemphys.2007.12.011.
- [13] M. Schwell, F. Dulieu, H.W. Jochims, J.L. Chotin, H. Baumgärtel, S. Leach, in: *Frontiers of Life, Proc. Xth Rencontres de Blois* (2000), The Goioi Publishers, Vietnam, 2003, p. 53.
- [14] A. Hoxha, R. Locht, B. Leyh, D. Dehareng, K. Hottmann, H.W. Jochims, H. Baumgärtel, *Chem. Phys.* 260 (2000) 237.
- [15] M.J. Frisch, G.W. Trucks, H.B. Schlegel, G.E. Scuseria, M.A. Robb, J.R. Cheeseman, J.A. Montgomery Jr., T. Vreven, K.N. Kudin, J.C. Burant, J.M. Millam, S.S. Iyengar, J. Tomasi, V. Barone, B. Mennucci, M. Cossi, G. Scalmani, N. Rega, G.A. Petersson, H. Nakatsuji, M. Hada, M. Ehara, K. Toyota, R. Fukuda, J. Hasegawa, M. Ishida, T. Nakajima, Y. Honda, O. Kitao, H. Nakai, M. Klene, X. Li, J.E. Knox, H.P. Hratchian, J.B. Cross, C. Adamo, J. Jaramillo, R. Gomperts, R.E. Stratmann, O. Yazyev, A.J. Austin, R. Cammi, C. Pomelli, J.W. Ochterski, P.Y. Ayala, K. Morokuma, G.A. Voth, P. Salvador, J.J. Dannenberg, V.G. Zakrzewski, S. Dapprich, A.D. Daniels, M.C. Strain, O. Farkas, D.K. Malick, A.D. Rabuck, K. Raghavachari, J.B. Foresman, J.V. Ortiz, Q. Cui, A.G. Baboul, S. Clifford, J. Cioslowski, B.B. Stefanov, G. Liu, A. Liashenko, P. Piskorz, I. Komaromi, R.L. Martin, D.J. Fox, T. Keith, M.A. Al-Laham, C.Y. Peng, A. Nanayakkara, M. Challacombe, P.M.W. Gill, B. Johnson, W. Chen, M.W. Wong, C. Gonzalez, J.A. Pople, *GAUSSIAN 03*, Revision C.02, Gaussian, Inc., Wallingford, CT, 2004.
- [16] Landolt-Bornstein, K.-H. Hellwege, A.M. Hellwege (Eds.), *Structure Data of Free Polyatomic Molecules*, vol.7, Springer-Verlag, Berlin, 1976, p. 177.
- [17] J.L. Derissen, *J. Mol. Struct.* 7 (1971) 67.
- [18] C.C. Costain, *J. Chem. Phys.* 29 (1958) 864.
- [19] D.W. Turner, C. Baker, A.D. Baker, C.R. Brundle, *Molecular Photoelectron Spectroscopy*, Wiley-Interscience, London, 1970.
- [20] G. Bieri, E. Heilbronner, V. Hornung, E. Kloster-Jensen, J.P. Maier, F. Thommen, W. von Niessen, *Chem. Phys.* 36 (1979) 1.
- [21] L. Åsbrink, W. von Niessen, G. Bieri, *J. Electron. Spectros. Relat. Phenom.* 21 (1980) 93.
- [22] P. Baybutt, M.L. Guest, I.H. Hillier, *Mol. Phys.* 25 (1973) 1025.
- [23] R.F. Lake, H. Thompson, *Proc. Roy. Soc. A317* (1970) 187.
- [24] K. Kimura, S. Katsumata, Y. Achiba, T. Yamazaki, S. Iwata, *Handbook of HeI Photoelectron Spectra of Fundamental Organic Molecules*, Halstead Press, New York, 1981.
- [25] F. Edard, A.P. Hitchcock, M. Tronc, *J. Phys. Chem.* 94 (1990) 2768.
- [26] A.P. Hitchcock, M. Tronc, A. Modelli, *J. Phys. Chem.* 93 (1989) 3068.
- [27] D.B. Beach, C.J. Eyermans, S.P. Smit, S.F. Xiang, W.L. Jolly, *J. Am. Chem. Soc.* 106 (1984) 536.
- [28] L.C. Snyder, H. Basch, *Molecular Wave Functions and Properties: Tabulated from SCF calculations in a Gaussian Basis Set*, Wiley, New York, 1973.
- [29] T.-K. Ha, *J. Mol. Struct.* 11 (1972) 185.
- [30] W.L. Jorgensen, L. Salem, *The Organic Chemist's Book of Orbitals*, Academic Press, New York, 1973.
- [31] T. Fujikawa, T. Ohta, H. Kuroda, *Chem. Phys. Lett.* 28 (1974) 433.
- [32] T. Fujikawa, T. Ohta, H. Kuroda, *Bull. Chem. Soc. Jpn.* 49 (1976) 1486.
- [33] C. Fridh, *J. Chem. Soc., Faraday Trans. II* 74 (1978) 2193.
- [34] M. Gochel-Dupuis, J. Delwiche, M.-J. Hubin-Fraskin, J.E. Collin, F. Edard, M. Tronc, *J. Am. Chem. Soc.* 112 (1990) 5425.
- [35] S. Eden, P. Limão-Vieira, P. Kendall, N.J. Mason, S.V. Hoffmann, S.M. Spyrou, *Eur. Phys. J. D26* (2003) 201.
- [36] R. Rianda, R.P. Frueholz, A. Kuppermann, *J. Chem. Phys.* 80 (1984) 4035.
- [37] G. Herzberg, *Molecular Spectra and Molecular Structure III. Electronic Spectra and Electronic Structure of Polyatomic Molecules*, Van Nostrand Reinhold, New York, 1966.
- [38] J.A. Nuth, S. Glicker, *J. Quant. Spectrosc. Radiat. Transfer* 28 (1982) 223.
- [39] K. Kanda, T. Nagata, T. Ibuki, *Chem. Phys.* 243 (1999) 89.
- [40] G. Herzberg, G. Scheibe, *Z. Phys. Chem.* B7 (1930) 390.
- [41] J.A. Cutler, *J. Chem. Phys.* 16 (1948) 136.
- [42] M. Suto, L.C. Lee, *J. Geophys. Res.* 90 (1985) 13037.
- [43] M. Gochel-Dupuis, J. Delwiche, M.-J. Hubin-Fraskin, J.E. Collin, *Chem. Phys. Lett.* 193 (1992) 41.
- [44] E. Lindholm, *Ark. Phys.* 40 (1969) 97.
- [45] M.B. Robin, *Higher Excited States of Polyatomic Molecules*, vol. III, Academic Press Inc., London, 1985.
- [46] D.M. Rider, G.W. Ray, E.J. Darland, G.E. Leroi, *J. Chem. Phys.* 74 (1981) 1652.